MAGNITUDE ESTIMATION BY THE NON-PACINIAN I TACTILE CHANNEL

by

Şeref Mete Dinçer

B.S., Chemical Engineering, Boğaziçi University, 2005

Submitted to the Institute of Biomedical Engineering in
partial fulfillment of the requirements
for the degree of
Master of Science
in
Biomedical Engineering

Boğaziçi University
June 2007

MAGNITUDE ESTIMATION BY THE NON-PACINIAN I TACTILE CHANNEL

APPROVED BY:

Assist. Prof. Dr. Burak Güçlü (Thesis Advisor)	……
Prof. Dr. Reşit Canbeyli	…….
Prof. Dr. Ahmet Ademoğlu	……..

DATE OF APPROVAL : 07 June 2007

ACKNOWLEDGMENTS

I would like to thank my advisor Assist. Prof. Dr. Burak Güçlü for his support, his patience and help at every step of this study.

I would like to thank TUBİTAK BİDEB for their financial support throughout my Master's study.

I would like to thank my subjects who showed great patience.

I would like to thank someone very special to me for her complimentary support during these two years.

Most importantly, I want to thank my mom, dad and my brother who lives far away for being a great family to me, and it's an honor to mention their gratuitous and unconditional support in my whole life.

ABSTRACT

MAGNITUDE ESTIMATION BY THE NON-PACINIAN I TACTILE CHANNEL

Psychophysical responses to mechanical stimuli were measured to study the sense of touch. By using a forward-masking procedure on eight subjects, magnitude estimation was performed by activating the Non-Pacinian I tactile channel. For each subject, 40-Hz and 250-Hz absolute thresholds were found. Additionally, the 250-Hz masking stimuli that were required to mask the Pacinian channel for selectively activating the Non-Pacinian I channel were determined. The masking stimuli were applied before the test stimuli to find the masked thresholds at 40 Hz. In the final set of experiments, supra-threshold stimuli were used to find magnitude estimation values. These values fit power functions well. Experimental results were compared to neural simulated population responses to study the origins of the power law. The model simulations that used the total number of spikes as the intensity code predicted the experimental results better.

Keywords: somatosensory, mechanoreceptor, power law, masking, Meissner corpuscles

ÖZET

PACINI-OLMAYAN I. DOKUNMA KANILINDA ŞİDDET ALGILAMA

Dokunma duyusunun işleyişini anlamak için mekanik uyarılara karşı psikofiziksel cevap ölçülmüştür. Bu çalışmada, maskeleme işlemi kullanılarak, 8 denek üzerinde, Pacini-olmayan I. psikofiziksel dokunma kanalında şiddet tahmini yapılmıştır. Her denek için 40 Hz ve 250 Hz'te eşik değerleri bulunmuş, Pacini kanalını maskeleyerek Pacini-olmayan I. kanalı izole etmek için gereken 250 Hz'lik maske uyarıları belirlenmiş ve elde edilen maske seviyeleri kullanılarak 40 Hz'te maskelenmiş eşikler elde edilmiştir. Son aşamada yapılan şiddet tahmini sonuçlarının psikofiziksel kuvvet fonksiyonuna uyduğu görülmüştür. Deneysel ölçümler sonucunda elde edilen değerler hesaplamalı nöron popülasyonu modelleriyle de kıyaslanarak kuvvet yasasının temelleri araştırılmıştır. Toplam sinir darbesi kullanan model simülasyonunun deney sonuçları ile daha iyi bir uyum gösterdiği bulunmuştur.

Anahtar Sözcükler: beden duyusu, mekanoreseptör, kuvvet yasası, maskeleme, Meissner cisimcikleri

TABLE OF CONTENTS

LIST OF FIGURES

LIST OF TABLES

LIST OF SYMBOLS

A_M	Amplitude in micrometers
A_{masker}	Amplitude value of the masking stimulus
$A_{threshold}$	Amplitude value of the threshold
D_M	Distance Metric
P	Probability value in statistical test
p	Detection proportion
α	Power function exponent

LIST OF ABBREVIATIONS

Att	Computer attenuation in decibels
DCN	Dorsal Column Nuclei
dB	Decibels
FA	Fast Adapting
LED	Light Emitting Diode
NIH	National Institute of Health
NP	Non-Pacinian
P	Pacinian
PC	Pacinian Corpuscle
RA	Rapidly Adapting
RF	Receptive Field
SA	Slowly Adapting
SL	Sensation Level
Stdev	Standard Deviation
StError	Standard Error

1. INTRODUCTION

1.1 Psychophysics and Magnitude Estimation

Psychophysics is the scientific study of the relation between stimulus and sensation, and therefore the problems of psychophysics constitute some of the most fundamental problems of modern physiology [1]. Scientists are trying to build robotic systems that can imitate the humans in many ways and they are conducting many clinical studies on human sensory systems which makes psychophysical investigations even more important in today's world.

Recent advancements in the study of tactile sensation have enabled scientists to study the system function in threshold and suprathreshold levels. Threshold studies yield information about the sensitivity of receptor mechanisms; however, information about the total range of tactile functioning is not obtained by threshold studies. In order to gain more knowledge on the functioning of tactile sensory system suprathreshold subjective scaling of vibrotactile stimuli are needed. One of the primary modes is the magnitude estimation method [2].

1.2 Hypothesis

The goal of this study is to obtain psychophysical magnitude functions of the Non-Pacinian I channel, which is isolated with masking stimuli. Generally, psychophysical relationships are best described by a power function [3] and until now, psychophysical studies using magnitude estimation task resulted with power functions of the form $R = kS^{\alpha}$ where R is the subject's response, S is the stimulus and α is the power function exponent [2, 4-7]. However, none of the studies have used masking procedures and magnitude estimation task specifically for the Non-Pacinian I channel of the tactile system.

My first hypothesis is that the magnitude estimation by the isolated Non-Pacinian I channel will also yield a power function. Each subject is expected to have power functions, but with different power-function exponents and constants.

Furthermore, experimental results may be related to the predictions of the population response model of the rapidly adapting fibers [8]. This is a probabilistic model in which various types of spatial distributions (Gaussian, uniform or rectangular) of the mechanoreceptors in the glabrous skin are compared by studying several parameters. Among these parameters, number of active rapidly-adapting fibers at a certain stimulus level is particularly important. Since, an increase in the number of active fibers suggests higher stimulus levels, the experimental results of magnitude estimation is expected to be represented by the number of active rapidly-adapting fibers. Most importantly, this relation might be in terms of the power law. Therefore, my second hypothesis is that the number of active tactile fibers is the intensity code used for magnitude estimation.

2. RELATED THEORY OF PSYCHOPHYSICS AND TOUCH

2.1 Historical Background

For centuries thinkers have recognized the importance of understanding sensation. In fact, experimental psychology developed as an independent science because of the recognition that the scientific study of sensation could yield insight into how the human mind works. Gustav Theodor Fechner founded psychophysics in 1860 with the publication of *Elemente der Psychophysik*. Fechner wanted to develop a theory that could relate matter to the mind, by describing the relationship between the world and the way humans perceive it. He described methods and theory for the measurement of sensation and gave basic psychological tools for the study of mind. Wilhelm Wundt, the founder of the first laboratory for psychological research, built upon Fechner's work [1].

2.2 Physiology and Anatomy of the Skin

The sensory receptors responsible for tactile sensations reside in the skin, a multilayered organ covering the entire body. The skin functions in thermoregulation, protection, metabolic functions and sensation. Sensory perception is critically important in the avoidance of pressure, mechanical or traumatic forces and extremes of temperature. Numerous specialized structures are present in the skin to detect various stimuli [9].

The skin is a highly complex structure, it includes sensory receptors and nerve fibers, blood vessels, sweat glands, and other specialized components such as hair, hoofs, claws, and nails. Skin can be classified into three types, glabrous or hairless skin characterized by the skin of the palm; hairy skin which includes hair; and mucocutaneous skin which borders the entrances to the body’s interior. These three types of skin have differences in their mechanical properties [9].

Skin has an outer layer (epidermis) and an inner layer (dermis). The below Figure 2.1 shows the three dimensional view of skin with the dermis and epidermis clearly indicated.

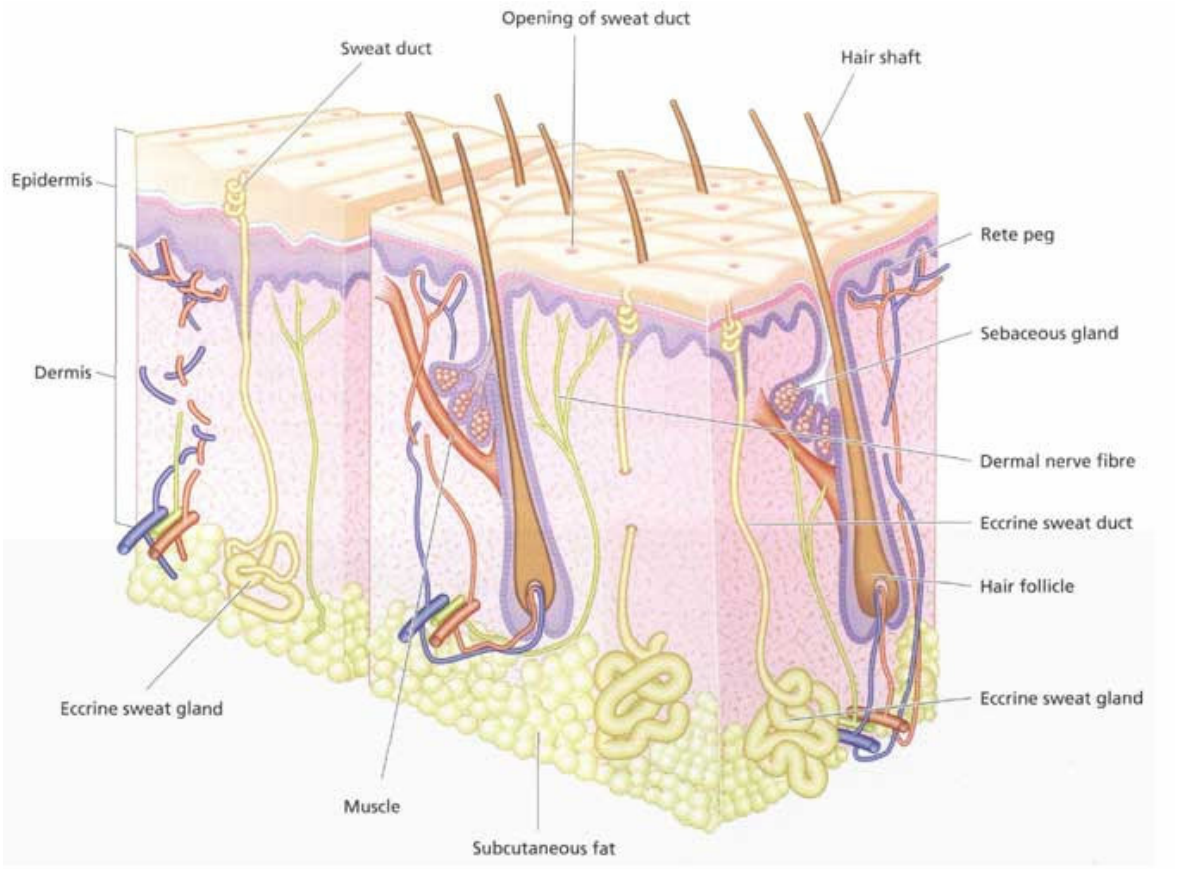

Figure 2.1 The three-dimensional structure of the skin [10].

The epidermis consists of stratified squamous epithelial cells in various stages of differentiation. The outermost layer, stratum corneum, is composed of dead cell tissue of a tough, horny nature. Epidermal cells are made in the lowest layer, the stratum germinativum (or basal layer), and migrate outwardly, reaching the stratum corneum where they die. The epidermis contains no blood supply [11].

The dermis is composed of connective tissue and elastic fibers floating in a semifluid, nonfibrillary amorphous mixture called the ground substance. Also embedded in the ground substance are fat cells, smooth muscle, sweat glands, and a profuse blood and

lymphatic supply. The dermis is composed of two layers, the papillary layer and the reticular layer [11].

2.3 Mechanoreceptors

The peripheral basis of tactile sensations arises by the activation of sensory receptors, located in the skin, that are responsive to mechanical stimuli. These sensory receptors are typically complex in structure, but the basic organization is that of a neuron that has unmyelinated terminal ending responsible for mechano-electric conversion.

Neural activity arising in the spinal nerves as a result of mechanical stimulation of the mechanoreceptors is passed across the dorsal root ganglion and enters the spinal column, where it takes one of the three routes. Following the first pathway, the activity is directly passed upward in the spinal column via tracts called the dorsal columns. These bilateral dorsal columns are myelinated fiber tracts in posterior region of the spinal cord. It is a direct pathway of activity to brain structures called the dorsal column nuclei (DCN), located in the brain stem. Since it is a direct pathway, no synapse is present between the site of mechano-electric conversion and the dorsal column nuclei. The synapses are located within the dorsal column nuclei and the projection neurons from the dorsal column nuclei are considered the second-order neurons of the somatosensory system. These secondary neurons form a pathway called the medial-lemniscal system, which projects directly to thalamus. The second pathway for the activity arising in the mechanoreceptor originates in the synaptic regions within the spinal cord, the central grey matter. Via a single synapse, the neural activity is relayed towards the brain by a pathway called the spino-cervical-thalamic tract. This pathway originates in spinal column, projects to the cervical nucleus and after synapsing there, the projection neurons merge with the dorsal-column/medial lemniscal system, subsequently synapsing in the thalamus. The third pathway does not go higher, central nervous system regions like thalamus, but operates at the spinal-cord level to control the responses of motor neurons (See Figure 2.2).

Information arising from the mechanoreceptors goes to specific regions within the thalamus, specifically the posterior and ventral-medial aspects. Processing of information

occurs at the level of the thalamus, and its output goes to primary and secondary somatosensory cortex [9, 12]. The first pathway described above is responsible for the tactile processing studied in this thesis.

The mechanoreceptor's neural component typically consists of an unmyelinated nerve terminal continuous with a myelinated nerve fiber, which has its soma in the dorsal root or trigeminal ganglion. The unmyelinated nerve terminal is the region where mechanotransduction takes place, whereas the myelinated nerve fiber is capable of transmitting action potentials [9, 12].

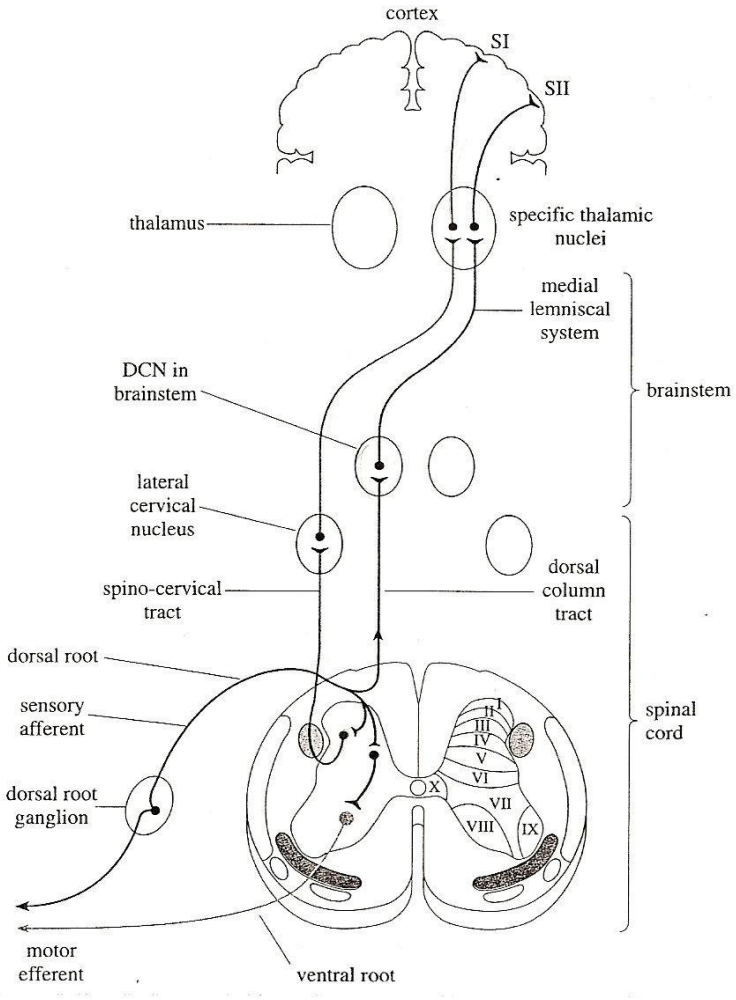

Figure 2.2 An overall view of the tactile pathways [9].

2.4 Vibrotactile Thresholds

Psychophysicists usually employ experimental stimuli that can be objectively measured, such as pure tones varying in intensity, or lights varying in luminance. All the senses have been studied: *vision, hearing, touch, taste, smell, and the sense of time*. Regardless of the sensory domain, there are three main topics in the psychophysical classification scheme: absolute thresholds, discrimination thresholds, and scaling [13].

A threshold (or limen), is the point of intensity at which the participant can just detect the presence of, or difference in, a stimulus. Stimuli with intensities below the threshold are considered not detectable, however stimuli at values close to threshold will often be detectable some proportion of the time. Due to this, a threshold is considered to be the point at which a stimulus, or change in a stimulus, is detected some proportion *p* (75% in the experiments described here) of the time [13].

2.5 Information Processing Channels

Fundamental to understanding the properties of sensory systems is the concept of an information-processing channel. A channel is made up of all the neural elements that are tuned to a specific feature of the stimuli system responds. Four information-processing channels (corresponding to four physiological receptors of tactile sensation) are thought to mediate the sense of touch. The thresholds of the channels are shown as a function of stimulus frequency in the below Figure 2.3 [14, 15].

Each channel represents a certain receptor subsystem of the tactile system. These receptors, namely, are Meissner receptors (NP I channel), Paccini corpuscles (P channel), Ruffini endings (NP II channel) and Merkel neurite complexes (NP III channel). The below Figure 2.3 shows the thresholds of the four channels. Threshold is defined as the magnitude of a vibratory stimulus required to induce a minimal sensation. Therefore, according to the figure, at around 250 Hz the most sensitive channel is the P channel. However, to induce sensation in other channels at the same frequency, the displacement must be increased. Similarly, at around 40 Hz, the most sensitive channel is the NP I

channel. At lower frequencies, NP III channel, mediated by the Merkel neurite complexes, becomes the most sensitive.

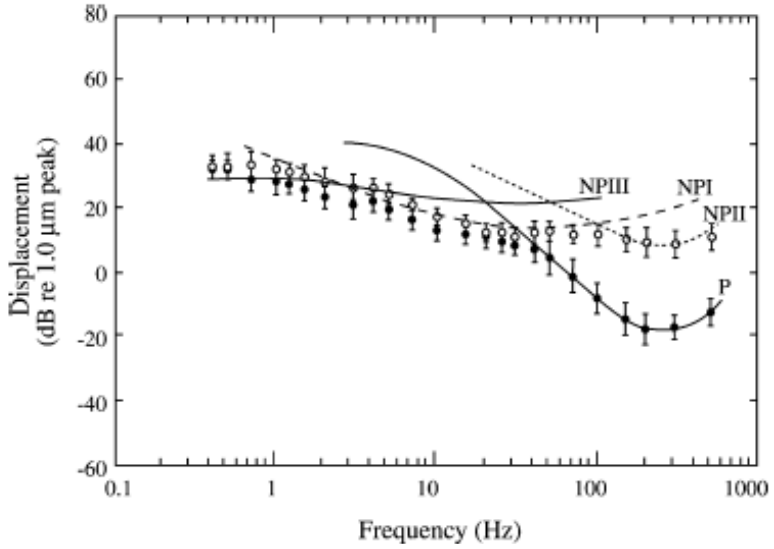

Figure 2.3 Stimulus-frequency curves of four tactile information-processing channels [15].

The threshold-frequency characteristics of the four channels were determined by means of manipulating stimulus parameters, such as the frequency and amplitude of the vibration, probe or contactor size, stimulus duration, skin-surface temperature, and the application of various masking techniques [16].

The mechanoreceptive afferent fibers are either fast adapting or slowly adapting. There are two subclasses to fast adapting and slowly adapting afferent fibers. The two principle features that define these four types are adaptational properties and receptive field size. Adaptation refers to how these afferents respond to sustained skin indentation. FA afferents respond while the skin is actively being indented, but do not generate action potentials when movement of the skin stops, even if the skin is still indented and force is exerted. SA afferents, in contrast, respond both while the skin is moving and during the period of sustained indentation, the discharge rate will slowly decrease in frequency as time passes. FA I (or RA fibers) mechanoreceptors respond mostly to the ramp portion of the stimulus while FA IIs (or PC) only respond to the fast transitions in the ramp-and-hold stimulus. SA Is, on the other hand, respond not only to the ramp portion of the stimulus, but also to the static portion with an irregular firing pattern. Finally, SA IIs display a more

regular firing rate and also have spontaneous activity, this activity occurs in the absence of mechanical stimulation [16].

The receptive field (RF) of a mechanoreceptor is the area of the skin that, when stimulated, will actuate the sensory neuron. The precise boundary of this area will depend upon the intensity of the stimulus used. But with a given stimulus level, the SA I and FA I afferents will be activated within a much smaller area of skin than the SA II and FA II afferents, which is to say that the type I fibers have smaller receptive fields than type II fibers (See Figure 2.4). Although adaptation and receptive field size are defining characteristics of the afferent types, there are other distinguishing features. Each of these four afferent types has been identified with a specialized structure within the skin: the FAI afferent with the Meissner corpuscle, the FAII afferent with the Pacinian corpuscle, the SAI with the Merkel cell-neurite complex, and the SAII with the Ruffini endings. Another important property is the innervation density of these receptors in the hand. Type I afferents (FAI and SAI) exhibit a large gradient of innervation; the greatest density found in the fingertips, becoming more sparse in the proximal direction. The Type II afferents show only a slight difference in density across the hand [16].

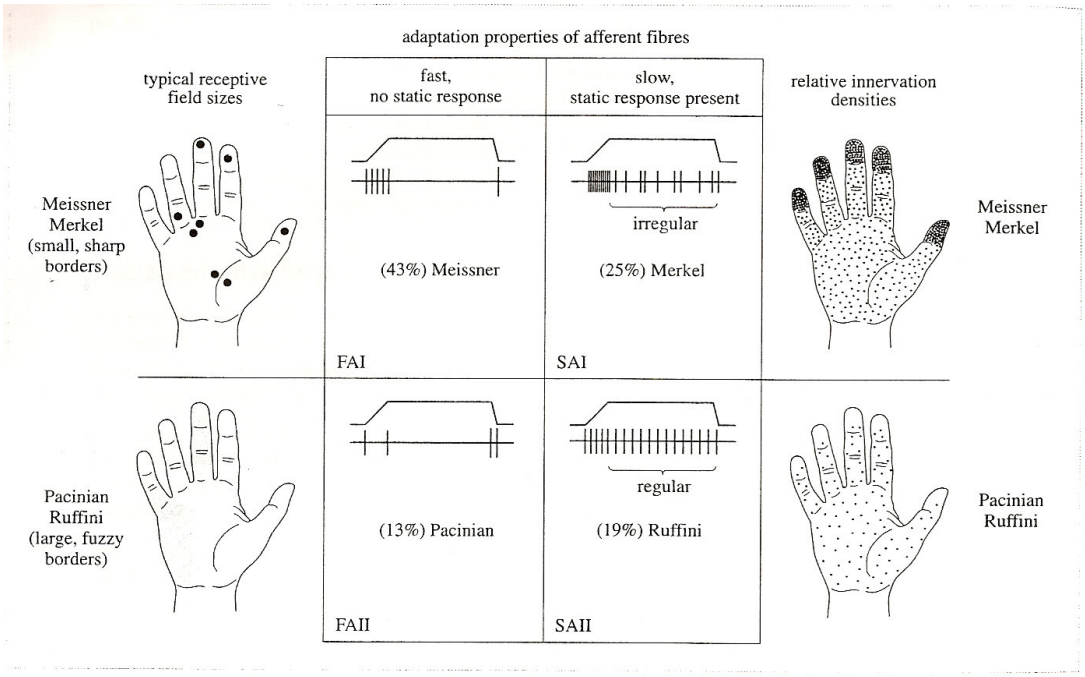

Figure 2.4 Characteristics of the four types of mechanoreceptive afferents that innervate the glabrous skin of the human hand. These characteristics are found using ramp-and-hold stimuli [9].

The percentages shown in the center of Figure 2.4 represent the relative frequencies of occurrence of the four afferent types and the most likely morphological correlate. One of the important response characteristics that help delineate the mechanoreceptor types is the rate-intensity charateristics. Rate-intensity characteristics define the relationship between action-potential firing rate and stimulus intensity. In general, the firing rates of mechanoreceptors increase with increasing stimulus intensity [9]. Thus, the intensity coding of magnitude estimation experiments performed in this thesis is also important and will be investigated by neural population response models.

2.6 Magnitude Estimation and Applications

2.6.1 Magnitude Estimation

Psychophysical ratio scaling method is the most frequently used method of magnitude estimation. In such an experiment, the observer is required to make direct numerical estimations of the sensory magnitudes produced by various stimuli. Stevens (1958) described two ways of applying magnitude estimation technique to a scaling problem. In the first one, the observer is presented with a standard stimulus and is told that the sensation it produces has a certain value (modulus), such as 10. On subsequent trials, observer assigns numbers to his/her sensations relative to the modulus. In the second method, no modulus is defined. So the observer is presented with random stimuli and expected to freely assign numbers to these stimuli related to their magnitudes [1].

2.6.2 Applications

Measurement of the physical properties on ratio scales has always been a highly desirable achievement, since these scales can contain the characteristics of order, distance, and origin while retaining maximal correspondence with the number system. Magnitude estimation has been used to investigate complex problems of how a sensory system functions. The method has become one of the most valuable tools for the study of sensory

processes and there have been many practical applications of magnitude estimation: to evaluate the analgesic effects of hypnosis, to measure clinical pain, to find relation of stress with secretion of epinephrine at different stress levels, to treat phobias, to relate drunkenness and alcohol concentration in blood, to establish reliability of diagnosis of the severity of mental disorders in psychotic patients and many more [1].

Magnitude estimation is characterized as a new method for directly measuring sensation and it provides an important basis for investigating the origins of a psychophysical law which gives the relation between intensity of stimuli and our impressions of them. Applying such a method in the experiments performed in this thesis and comparing to the neural population responses would give a better understanding of the human tactile system and would provide more proof on the presence of a psychophysical law. Thus, the above mentioned practical applications may psychophysically be modeled.

2.7 Modeling In Psychophysics

One of the fundamental issues in psychophysics concerns the form of the psychophysical law and the main concern is to discover a simple equation. In the presence of a psychophysical law, psychologists' theories and research on information processing would be influenced. Additionally, neurophysiologists' search for the mechanisms by which nervous system encodes environmental stimuli would be facilitated. Even social scientists may benefit from a psychophysical law such that some of the difficult problems about understanding human behavior in social environments may be simplified [1].

The first psychophysical law was proposed by G. T. Fechner. He was trying to solve the problem of how the inner world of sensation is related to the outer world of stimuli, and proposed a logarithmic function. In mid-1950s S. S. Stevens, using ratio scaling methods, obtained psychophysical magnitude functions for brightness and loudness that were did not resemble logarithmic functions. Eventually, the new form of relationship between sensation magnitude and stimulus intensity proposed by S. S. Stevens took place of Fechner's logarithmic law. This new form is known as the power function. Assuming

that the power law is correct, scaling problem becomes the experimental determination of the exponent of the power function.

As in many scientific studies mathematical models and computational simulations utilizing these models play an important role. In case of determining psychophysical responses, population response models of tactile afferent fibers are important. Early models did not include the large variability seen in the response properties of fibers, and they were improved by including statistical distributions of the response properties. Later, the effects of anatomical distribution of receptive fields on population response were also considered [17].

One of the assumptions made in the early modeling studies was the notion of symmetric receptive fields. No matter what the stimulus location is, equidistant fibers have identical responses. However, this requirement was not seen physiologically. This was partly due to the stochastic properties of nerve fibers. The exact form of the neural-response functions could be only defined in probabilistic terms. In one of the early studies Johansson and Vallbo (1980) constructed a graphical display of the distribution of RA and SA I mechanoreceptive unit responses. They attempted to show how a population of receptive fields may be activated due to a one- or two- point stimulus, under the assumptions of uniform-sized, circularly-shaped receptive fields distributed uniformly, but randomly. In another study, Johnson (1974) used sinusoidal stimulation. It was structured enough to be a basis for a testable model. Goodwin and Pierce (1981) modeled the response of an “average” RA-fiber population when two-probe contactor was used. There was no superposition of the amplitude of the two probes. The model used to in this thesis uses Johnson’s basic model and is relevant to the study of Goodwin and colleagues since they demonstrate that contribution of the dependence on the stimulus and fiber characteristics could be separated [8]. Furthermore, it considers temporal-response properties of tactile fibers that none of the above models do [17].

3. METHODOLOGY

3.1 Subjects

4 male and 4 female subjects with ages in the range of 22-26 participated in the experiments. Young adults were selected because vibrotactile sensitivity decreases with age [11]. The experiments adhere to NIH ethical guidelines for testing human participants and were approved by the Ethics Committee for Human Subjects of Boğaziçi University.

3.2 Apparatus

Stimuli generated by the computer were filtered by a custom-made 1 kHz low-pass filter, the electrical signal coming from the PC was attenuated by a digitally controlled attenuator (PA5, TDT Inc.) before amplified by a power amplifier (Alesis RA 300 Amplifier). The amplified stimuli were applied to the left middle fingertip by a V203 electro-dynamic shaker driving a contactor probe with 2 mm radius and without a contactor surround (Ling Dynamic Systems Ltd., Royston, Herts, UK). The shaker was mounted on horizontal metal rail and was vertically lowered to the fingertip. The vibrations generated by the shaker were measured by a LVDT (Lucas Control Systems, Pennsauken, NJ) and monitored with an oscilloscope. In order to prevent the movement of the fingertip, the finger was immobilized in modeling clay. The fingertip was also monitored by a CCD camera. The sound of the shaker was masked by continuous auditory noise applied with headphones. The response of the subject was obtained by a custom-made response box connected to the computer. The experiments were conducted in the psychophysics lab shown in Figure 3.1.

Figure 3.1 The subject booth (left) and the control room (right).

3.3 Software

A MatLab code controlled the PC to generate sine wave signals. The MatLab codes necessary to simulate and observe the first few experimental procedures (explained below) were already available. However, additional code was written to perform the magnitude estimation experiments (See Appendix A).

3.4 Stimuli

The stimuli were mechanical vibrations which started and ended as cosine-squared ramps of 50 ms rise/fall times. The duration of the test stimuli was 0.5 s both for the masked and unmasked experiments. The stimuli were burst of sine waves with varying amplitudes as shown in Figures 3.2 and 3.3. The interval between two stimuli was 2 seconds.

The stimulus was applied on the terminal phalanx of the middle finger. The length of the phalanx was measured before the experiment (the distance between the joint line and fingernail). The contact point was normalized as: (phalanx length)*1.5/3.5 cm from the joint line; and marked on the subject's finger with a felt-tip pen. This location approximates the center of the finger pad. The stimulus contactor probe was applied to this point.

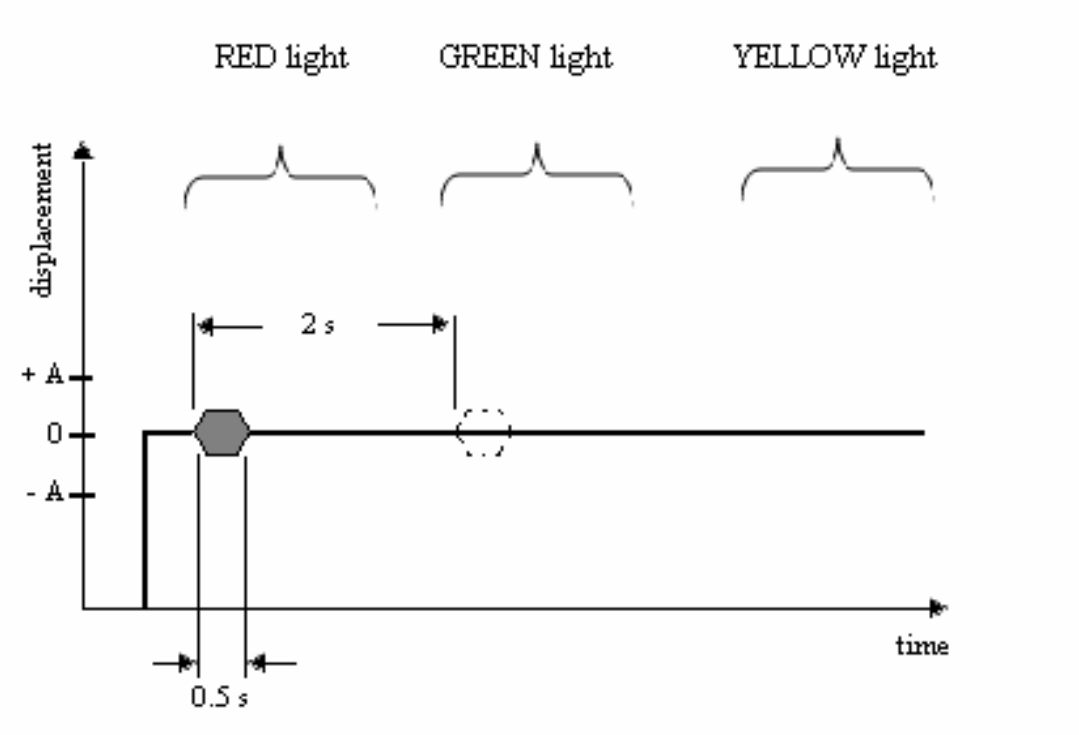

Figure 3.2 Stimulus timing diagram for the two-interval forced-choice task of measuring unmasked thresholds at 40 Hz and 250 Hz.

In early works, it had been shown that the thresholds were affected by static indentation [18, 19]. To ensure continuous contact with the skin during stimulation, the displacements were superimposed on a static indentation of 0.5 mm. The static indentation was adjusted by a micrometer after contact with the skin was achieved.

Masking-stimulus duration was 1 s with rise/fall times of 50 ms. The test stimulus was presented 150 ms after the masking stimulus. The interval between the two masking stimuli was 2 s. According to the literature, as the interval between the masking stimulus and the test stimulus increases the masking effect decreases. The time interval used between masking and test stimuli was long enough to induce the masking effect [18].

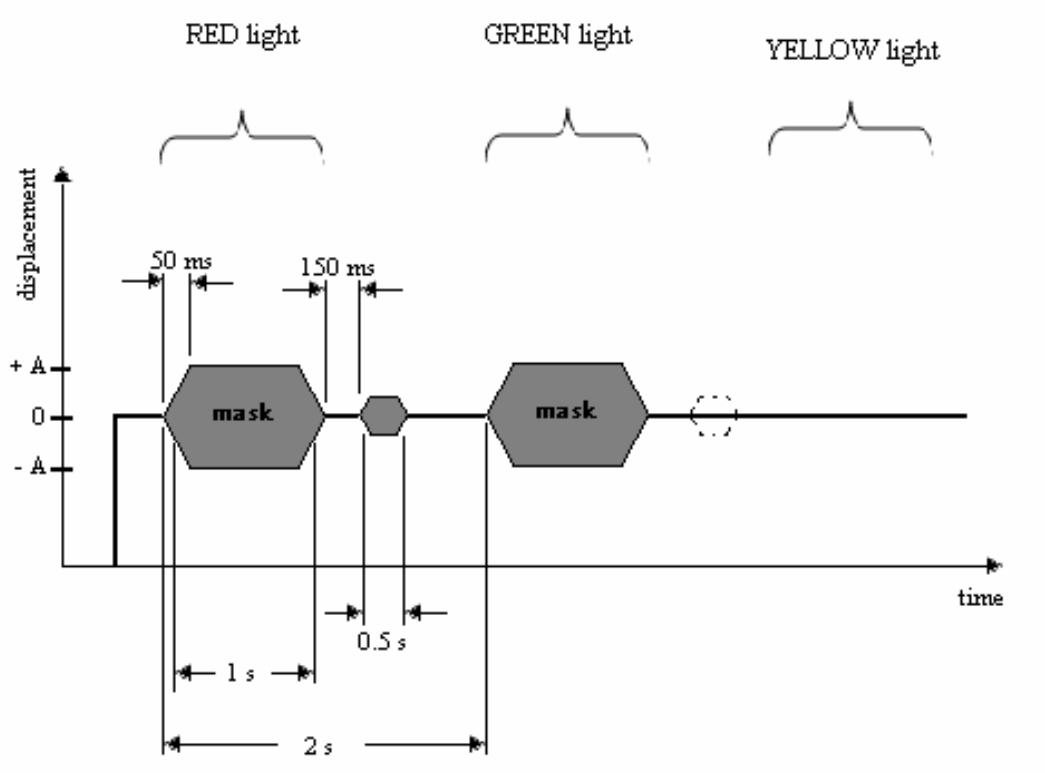

Figure 3.3 Stimulus timing diagram for masked-threshold experiments.

3.5 Experiments

The experiment was composed of three parts. In the first part, psychophysical thresholds (unmasked) of each subject were determined at two frequencies (40 Hz & 250 Hz). In the second part, the NP I channel was isolated at 40 Hz by masking the P channel at 250 Hz. In the third part, subjective magnitude estimation was performed for the NP I channel by using 40 Hz stimuli.

The variation in skin surface temperature can significantly affect vibratory sensitivity, especially for higher stimulus frequencies [11]. It is known that the subjective magnitude of vibration is affected by temperature in the Pacinian channel whereas no effect was seen in the NP I channel [7]. Since both P and NP I channels were important for this study, temperature of the finger was monitored and found to be between 32-36 ^{o}C.

3.5.1 Part 1

In all the psychophysical threshold experiments, the two-interval forced-choice task was used to obtain results independent of the subject's criterion. The stimulus levels were changed by an up-down rule [20]. This rule increases the level of stimulus by one step (1 dB) for each incorrect answer; and decreases one step (1 dB) for three correct answers (not necessarily consecutive). The threshold experiment was stopped when the subject's responses varied within $\pm$1 dB range for the last 20 trials. The stimulus level at the end of this procedure was recorded as the threshold. The time intervals of the two-interval forced-choice task were presented to the subject by red and green lights on the response box. At the end of each trial, a yellow light on the box signaled that a response is expected from the subject. In this part of the experiment, the subject's task was to decide whether the stimulus occurred in the first or the second interval. The stimulus-timing diagram is given in Figure 3.2. Each threshold measurement was repeated four times at a given frequency.

3.5.2 Part 2

In this part, 250 Hz stimuli were used to mask the P channel. Both the masking and test stimuli were at 250 Hz. This task was similar to the unmasked threshold experiment, but here, the threshold shift of the P channel was determined in the presence of a masking stimulus. Adequate threshold shift was obtained for the P channel by varying the masking-stimulus. Then, the 40 Hz threshold of the NP I channel was obtained by applying a 40 Hz test stimulus while masking the P channel. The dynamic range for activating the NP I channel was uniquely determined by subtracting the maximum masked threshold of the P channel from the NP I channel threshold. This procedure was performed for each subject individually. The stimulus-timing diagram is presented in Figure 3.3. Each measurement was repeated four times. The stimulus levels which caused decoupling between skin and probe were given in the literature [21]. In order to avoid such decoupling during the masking experiments, amplitudes smaller than 250 micrometer were used.

3.5.3 Part 3

In this part of the experiment, a visual magnitude estimation experiment was carried out to train the subjects. 10 lines at different lengths were shown 10 times to the subjects in random order (adds up to 100 visual stimuli). Subjects assigned numbers to different line lengths they perceived. Then, tactile magnitude estimation was performed at 250 Hz. 5 supra-threshold stimuli were presented 20 times in random order. Subjects assigned numbers to 250Hz test stimuli presented at different amplitudes (no forward masking is used). This task activated the P channel. Next, the NP I channel was activated by 40 Hz stimuli applied with forward masking. The subject assigned numbers, without a standard, to the subjective magnitudes of the 40 Hz test stimuli. The subjects were allowed to use any number, including decimals and fractions, except negative numbers. This method was established in the literature [22]. For every subject, 20 magnitude estimations were obtained for each stimulus level within the dynamic range of the NP I channel.

3.6 Measurement Conversions

At the end of each run a computer attenuation value was found. These attenuation values in dB were converted to displacement values in dB by the following calibration equations for 40 Hz and 250 Hz:

$$\text{40 Hz Calibration equation : } -1.0246 \times Att + 81.493 \tag{3.1}$$

$$\text{250 Hz Calibration equation : } -1.0162 \times Att + 58.140 \tag{3.2}$$

The calibrations were done by a photonic sensor (MTI Z100 Fotonic Sensor, MTI Instruments Inc.). Micrometer displacements corresponding to the displacements in decibels shown on the attenuator were measured. Eventually, calibration graphs were plotted and the above Equations 3.1 and 3.2 were obtained by linear fitting. Displacements obtained were converted to micrometers by the following formula:

$$A_M = 10^{(Displacement/20)} \tag{3.3}$$

For each subject (subjects are referred to between S1-S8), four different micrometer values were averaged and reconverted to displacement in dB, by applying the reverse of Eq. 3.3.

In Eq. 3.4, the amplitude values in parenthesis are in units of micrometers. The resulting unit for SL is in dB. So, sensation level for masking experiments is defined as follows:

$$SL = 20 \times \log\left(\frac{A_{mas\,\mathrm{ker}}}{A_{threshold}}\right) \tag{3.4}$$

Eq. 3.4 can simply be interpreted as the difference between the threshold and masking stimulus in dB units.

3.7 Modeling Approach

The model used to simulate the response of rapidly adapting fibers at 40 Hz is a stochastic model. According to the model, about 10 active fibers are required for the detection of a 40 Hz vibratory stimulus. Model simulations were performed for eight simulated subjects. Simulations were carried out four times for each simulated subject and the average of these four runs were taken. The experimental results were compared to simulation results with three intensity codes: number of active fibers, total number of spikes and maximum number of spikes. This model uses a tristate Markov process for spike generation [17].

In 1907, A. A. Markov began the study of an important new type of chance process. In this process, the outcome of a given experiment can affect the outcome of the next experiment. Using this analysis, one can generate a new sequence of random but related events, which will look similar to the original. This type of process is called a Markov chain [23].

A Markov chain is a series of states of a system that has the Markov property. At each time the system may have changed from the state it was in the moment before, or it may have stayed in the same state. The changes of state are called transitions. Markov chains have many applications in biological modelling, particularly population processes, which are useful in modelling processes that are analogous to biological populations [24, 25].

A Markov chain is described as follows: There is a set of *states,* $S = \{s_1, s_2, ..., s_r\}$. The process starts in one of these states and moves successively from one state to another. Each move is called a *step.* If the chain is currently in state s_i, then it moves to state s_j at the next step with a probability denoted by p_{ij}, and this probability does not depend upon which states the chain was in before the current state. The probabilities p_{ij} are called *transition probabilities.* The process can remain in the state it is in, and this occurs with probability p_{ii}. An initial probability distribution, defined on S, specifies the starting state. Usually this is done by specifying a particular state as the starting state [23].

The probabilities associated with the Markov model is supposed to match the firing statistics, or simply, the model should be based on these probabilities. Markov processes are not uncommon in computational neuroscience and they have been used in sensory systems other than touch [26].

Some mathematical relations used in the model that was simulated in this thesis are given below:

$$r = \begin{cases} 0; & 0 < A < a_0 \\ \dfrac{f_s}{a_1 - a_0}(A - a_0); & a_0 < A < a_1 \\ f_s; & a_1 < A < a_2 \\ f_s\left(1 + \dfrac{A - a_2}{a_3 - a_2}\right); & a_2 < A < a_3 \\ 2f_s; & a_3 < A \end{cases} \qquad \text{for } a_0 < a_1 < a_2 < a_3 \tag{3.5}$$

A is the effective stimulus amplitude, f_s is the stimulus frequency, r is the average firing rate and (a_0, a_1, a_2, a_3) are rate-amplitude-function parameters (from monkey). Equation 3.5, approximates rate-amplitude function of each tactile fiber. Each fiber's average firing rate calculated from the above equation becomes a nominal rate that is input to the Markov process [17].

$$\mathbf{p}(n+1) = \begin{bmatrix} p_{00} & p_{01} & p_{02} \\ p_{10} & p_{11} & p_{12} \\ p_{20} & p_{21} & p_{22} \end{bmatrix} \mathbf{p}(n) = P\mathbf{p}(n) \tag{3.6}$$

In Equation 3.6, P is the stochastic matrix of transition probabilities. p_{ij} stands for the probability of a transition from state i to state j. $p(n)$ is the vector of probabilities for each state at cycle n. After the probabilities are determined at each cycle of the stimulus, random generator of the computer is used to determine the next state of the simulated tactile fiber [17].

$$\rho = \left\{ \{o_k\}: \sum_k \mathbf{I}_{[1,\infty)}(|\{o_k\}|) > 9 \right\} \tag{3.7}$$

Equation 3.7 represents the rule for stimulus detection. It means that there should be at least ten active fibers so that the stimulus can be detected. ρ represents the decision rule, $\{o_k\}$ refers to the output of the population (for example; the set of spike times for each kth fiber) and $\mathbf{I}_{[...]}()$ is the indicator function which has the value of one if its argument belongs to the set indicated in the subscript, otherwise it is '0' [17].

3.8 Distance Metric

A novel distance metric was defined, in this thesis, to investigate the relation between two or more groups of data points which do not have statistical differences. The specific aim in defining such a metric was to decide which model simulation was closer to

the magnitude estimation data. This novel distance rule was explained below (see below Figures 3.4 and 3.5)

Figure 3.4 shows the shortest distance lines from each data point of the first group to the second group and similarly, Figure 3.5 shows the shortest distance lines from each data point of the second group to the first group. First, the nearest neighbor of each point in the first group was found in the second group. Then, the distances between the points in the first group and the nearest neighbors were averaged (see Eq. 3.8). This procedure is repeated to find the shortest distances from the second group to the first group.

$$D_M = \frac{d1 + d2 + ... + dn}{n} \tag{3.8}$$

The smallest of the two values found was used to decide which of the different models used in this thesis was closer to the experimental results. Smaller distance metric indicates that experimental and simulation results are close to each other.

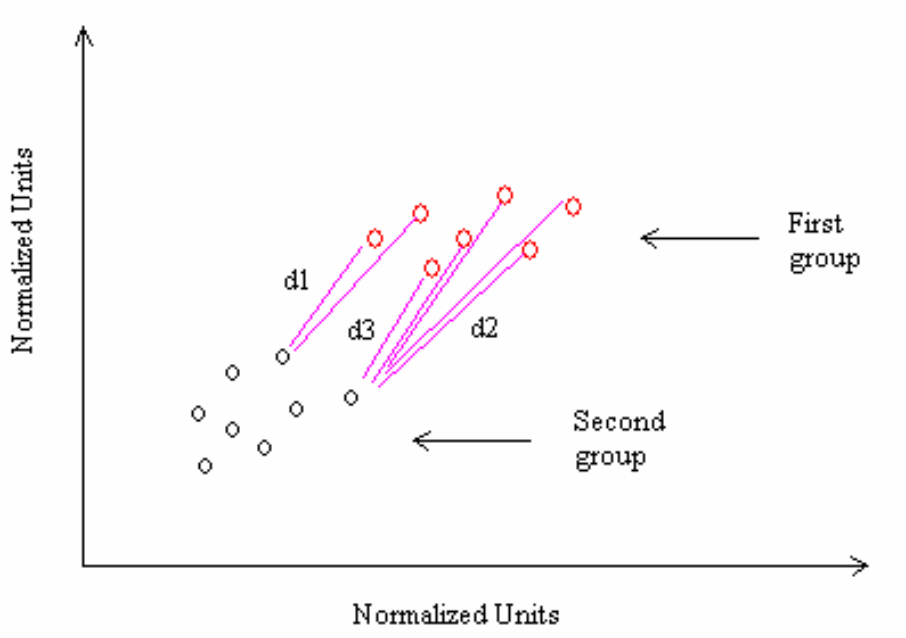

Figure 3.4 Shortest distances from data points of the first group to the second group.

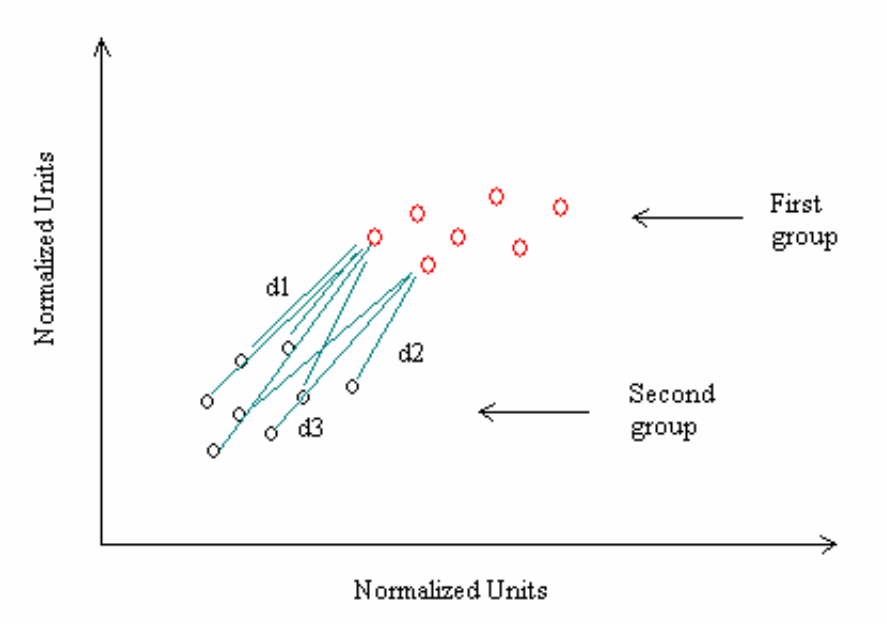

Figure 3.5 Shortest distances from data points of the second group to the first group.

4. RESULTS

4.1 Threshold Experiments

The thresholds for eight subjects were in the 3.6, 5.0, 9.5, 10.0, 11.7, 14.6, 15.1, 18.2 dB range at 40 Hz and in the -26.0, -19.7, -14.5, -10.6, -10.3, -9.8, -8.9, -5.4 dB range for 250 Hz (Figures 4.1 and 4.2). These results were compared to the results from literature [27] with a two-sample t-test and no differences were found (See Table 4.1).

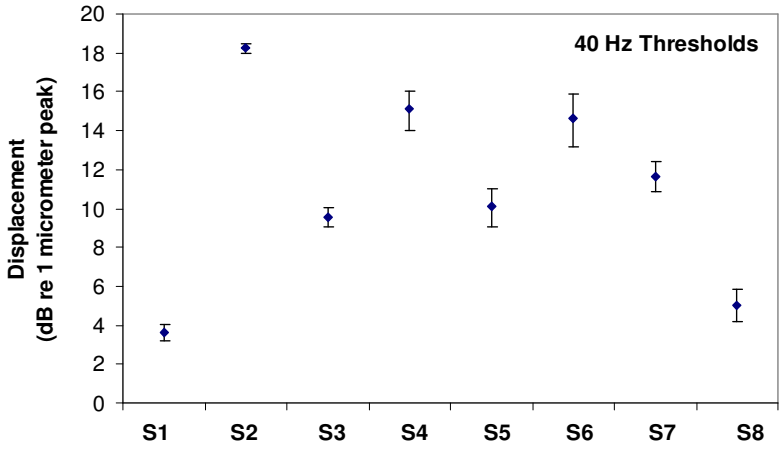

Figure 4.1 Thresholds at 40 Hz with reference to one micrometer peak displacement (Standard error bars are shown on data points).

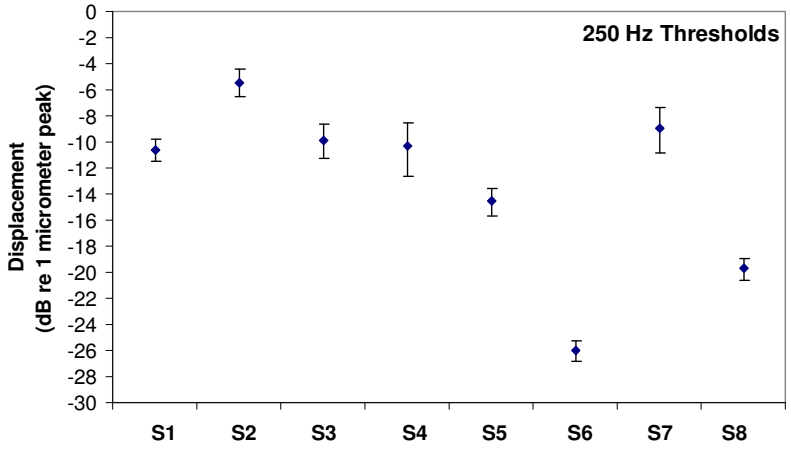

Figure 4.2 Thresholds at 250 Hz with reference to one micrometer peak displacement (Standard error bars are shown on data points).

Table 4.1
Statistical comparison of the results from eight subjects with results from similar experiments in the literature.

Statistical Comparison	Experimental Condition	Statistical test	Statistical result
Literature [27, 28] vs. Eight subjects	40 Hz unmasked	Two-sample *t*-test	P=0.59 (no significant difference)
Literature [27, 28] vs. Eight subjects	250 Hz unmasked	Two-sample *t*-test	P=0.63 (no significant difference)
Literature [27, 28] vs. Eight subjects	40 Hz masked	Two-sample *t*-test	P=0.79 (no significant difference)

4.2 Forward Masking and Masking Functions

Figure 4.3 shows the masking functions found for each subject. Both the masking and the test stimuli were at 250 Hz. The largest masking stimulus which did not cause decoupling between the skin and the probe was determined. As shown in Figure 4.3, an increase in masking level caused an increase in the threshold shift. For the proceeding experiments, the largest masking level obtained for each subject was used.

The x-axis of Figure 4.3 is the masking level referenced to the sensation level. According to Figure 4.3, as the sensation level increased the shift in threshold increased for every subject. At the end of masking experiment at 250 Hz, a line was fitted to the data points obtained for each subject. At the bottom right-hand corner of each graph, the masking functions obtained as the result of line fitting are shown. Goodness of fit values (R^2) are also shown. Line fits gave high goodness of fit values ($R^2 > 0.84$) except for three graphs with lower goodness of fit ($R^2 = 0.05$, 0.36 and 0.42).

Using the largest masking level shown in Figure 4.3, masked threshold at 40 Hz was obtained (See red dot in Figure 4.4). These results were compared to the results from the literature [27] with a two-sample t-test and no statistical differences were found (See Table 4.1). The dynamic range for selective activation of the NP I channel is shown in Figure 4.4. Some subjects had a wide range (between red & light blue data points) while some had smaller dynamic ranges.

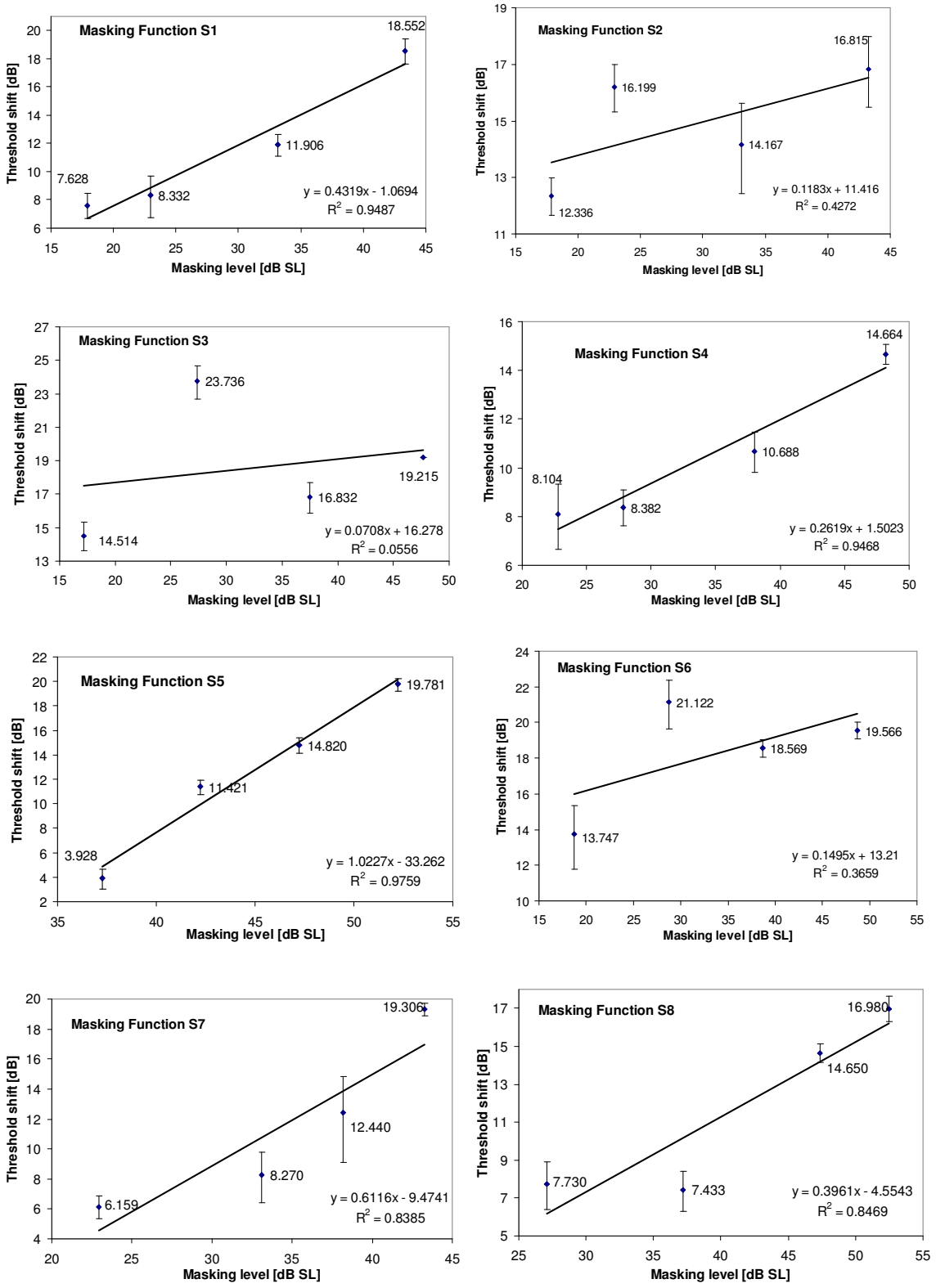

Figure 4.3 Resulting threshold shifts with respect to the unmasked thresholds at 250Hz are plotted as a function of the masking level. (Standard error bars are shown on data points).

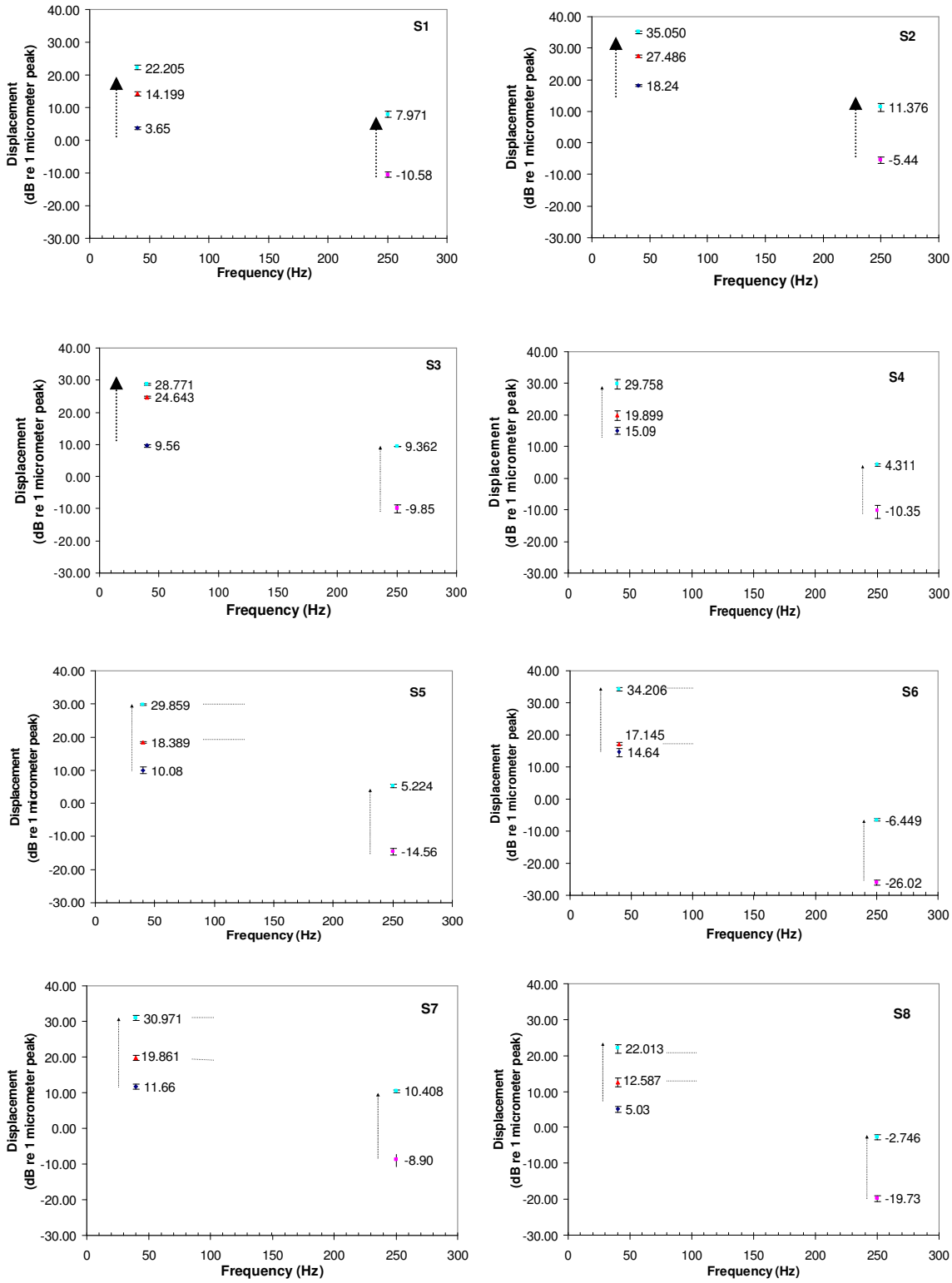

Figure 4.4 Unmasked thresholds, masked thresholds and threshold shifts at 40 Hz and 250 Hz. Arrows indicate the threshold shifts at 40 & 250 Hz frequencies resulting from masking at 250 Hz. Red dot at 40 Hz shows the masked threshold. The range between the top light blue dot and the middle red dot represents the dynamic range for selective activation of the NP I channel upon masking. (Standard error bars are shown on data points).

4.3 Magnitude Estimation Results

As shown in Figures 4.5 and 4.7, the results could be fitted by the power law. Since magnitude estimation results had great variation from subject to subject a normalization procedure was used. Grand average of all the responses was calculated for every subject. Then, average magnitude estimates obtained for different stimulus intensities were divided by this grand average. Therefore, magnitude estimation values of eight different subjects were brought to a comparable scale (See Figures 4.6 and 4.8).

The x-axes of Figure 4.5 and Figure 4.7 are the stimulus amplitude in micrometers. According to Figure 4.5, as the stimulus amplitude increased normalized magnitude estimations of all subjects increased. At the end of magnitude estimation experiment at 250 Hz, a power function was fitted to the data points obtained for each subject. At the bottom right-hand corner of each graph, the power functions obtained as the result of this fitting are shown. Goodness of fit values (R^2) are also shown. Power functions gave high goodness of fit values ($R^2 > 0.68$).

The results of magnitude estimation for the NP I channel (at 40 Hz masked) are shown for each subject in Figure 4.7, for all subjects in Figure 4.8. The power function exponents obtained at 250 Hz and 40 Hz are tabulated in Table 4.2. Table 4.2 also shows the power function exponents and their average obtained at the end of line length estimations. The average power function exponent of line length estimation in the literature [29] was 0.90 whereas the average exponent obtained in this study was 0.98. The one-sample t-test resulted with a value of P = 0.32. Therefore, power function exponents of the line length estimation were not statistically different from the literature value [29]. The difference between the exponents for NP I and P channels was statistically significant (P=0.02; See Table 4.3). However, there was no statistical difference between male and female subjects regarding the power exponents (See Table 4.3).

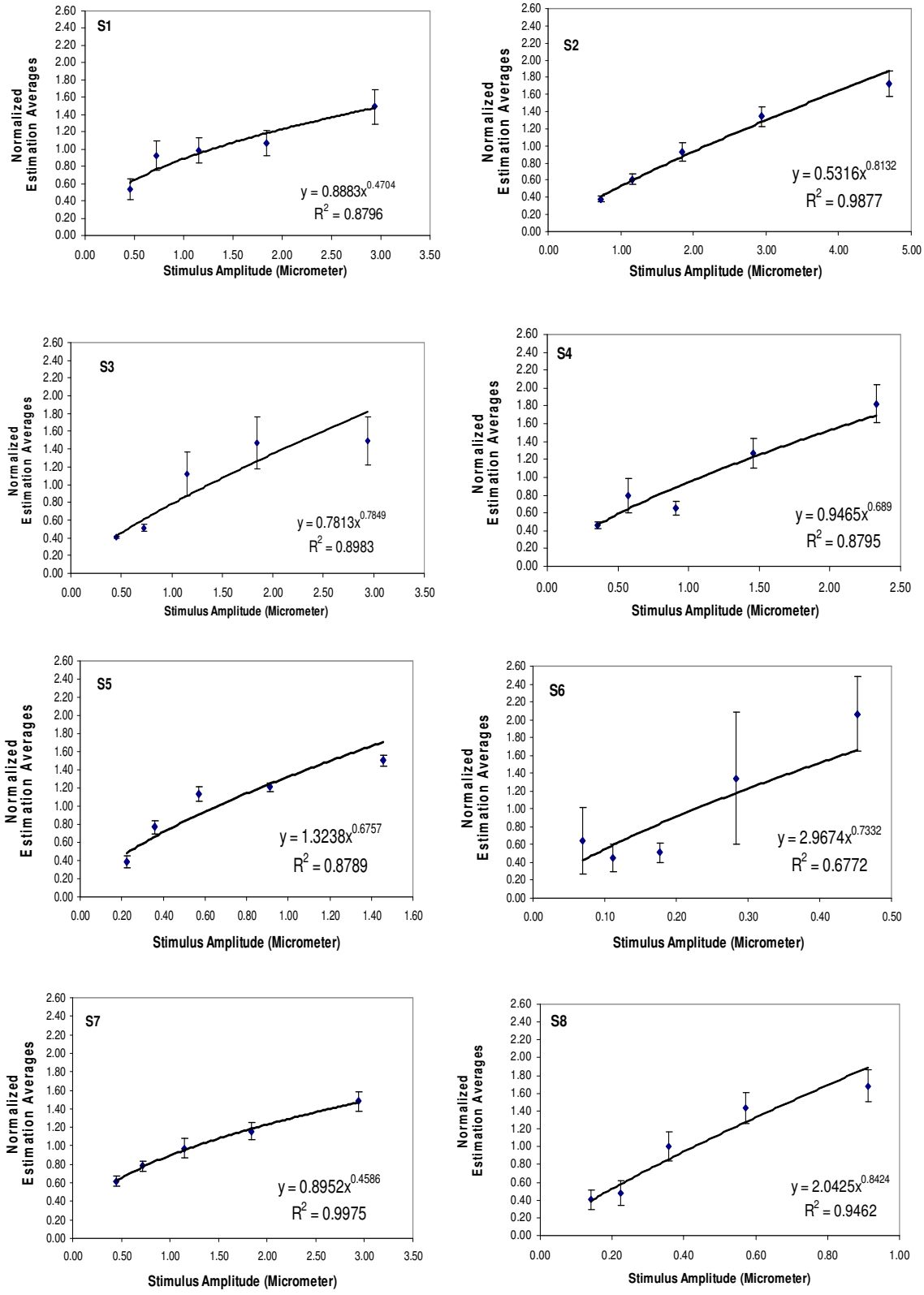

Figure 4.5 Normalized magnitude estimation values for the Pacinian channel. Horizontal axis shows the displacement in micrometer at 250 Hz. The power functions fitted to the data points are also given. (Standard error bars are shown on data points).

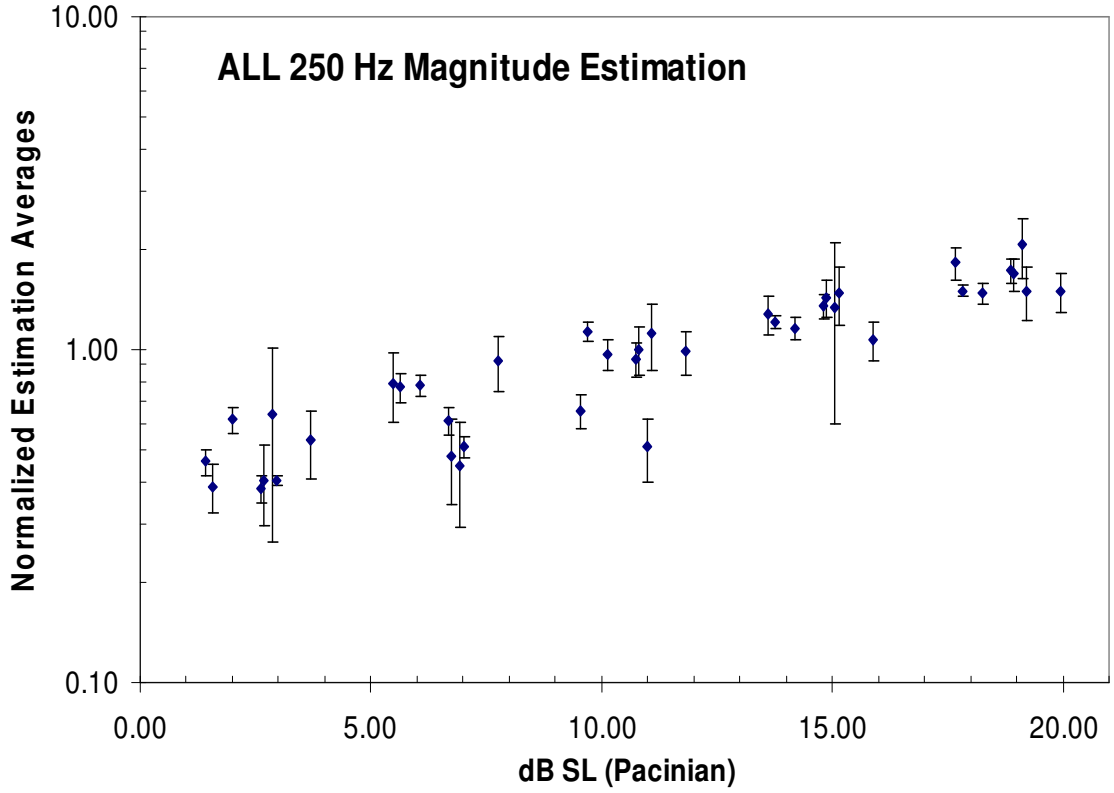

Figure 4.6 Normalized magnitude estimation values for the Pacinian (P) channel (250Hz unmasked) of all subjects. Horizontal axis is the stimulus level referenced to threshold. (Standard error bars are shown on data points).

According to Figure 4.7, as the stimulus amplitude increased normalized magnitude estimations of all subjects increased. At the end of magnitude estimation experiment at 40 Hz, a power function was fitted to the data points obtained for each subject. At the bottom right-hand corner of each graph, the power functions obtained as the result of this fitting are shown. Goodness of fit values (R^2) are also shown. Power functions gave high goodness of fit values ($R^2 > 0.93$).

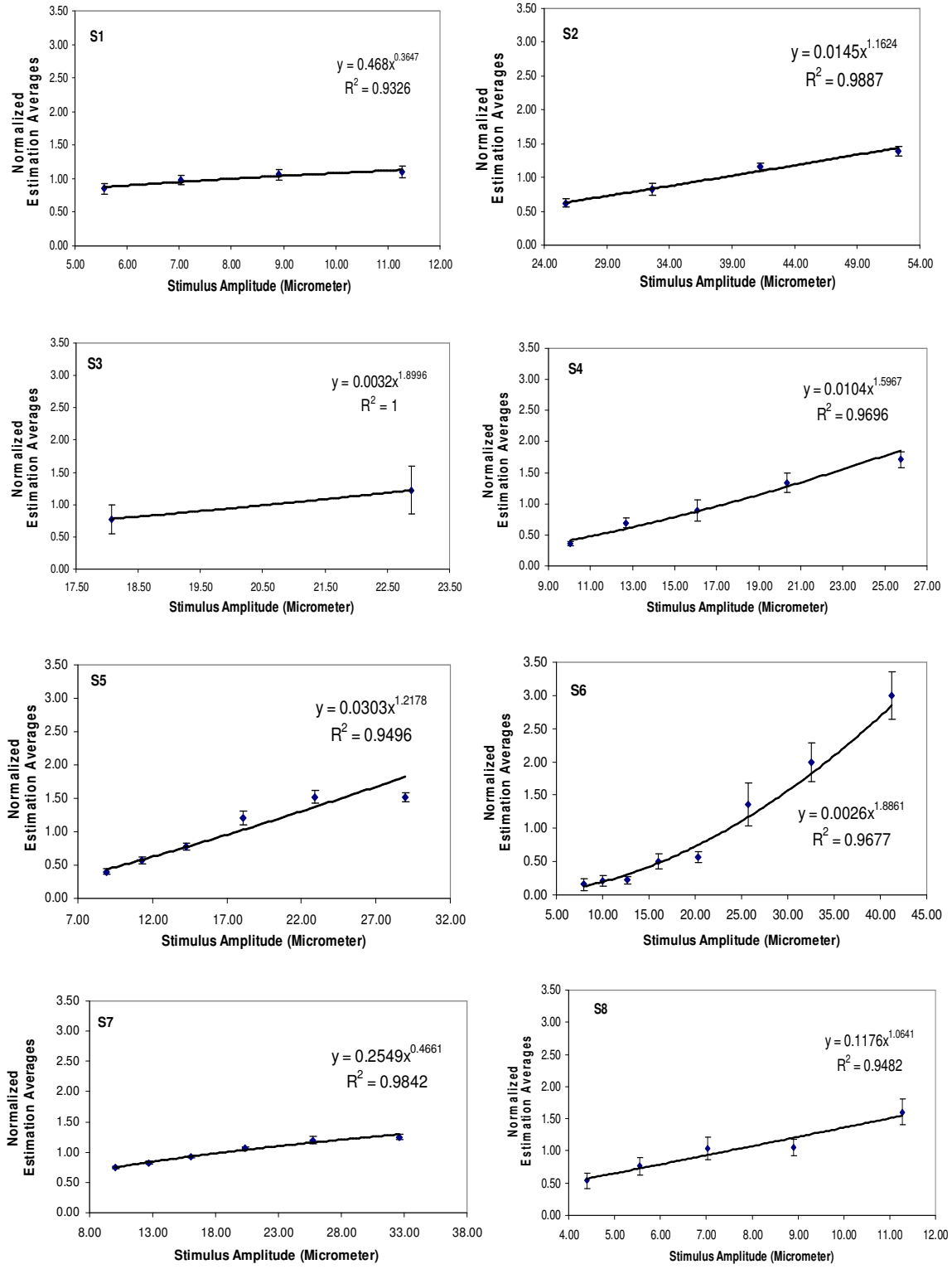

Figure 4.7 Normalized magnitude estimation for the NP I channel. Horizontal axis shows the displacement in micrometers at 40 Hz. The power functions fitted to the data points are also given. (Standard error bars are shown on data points).

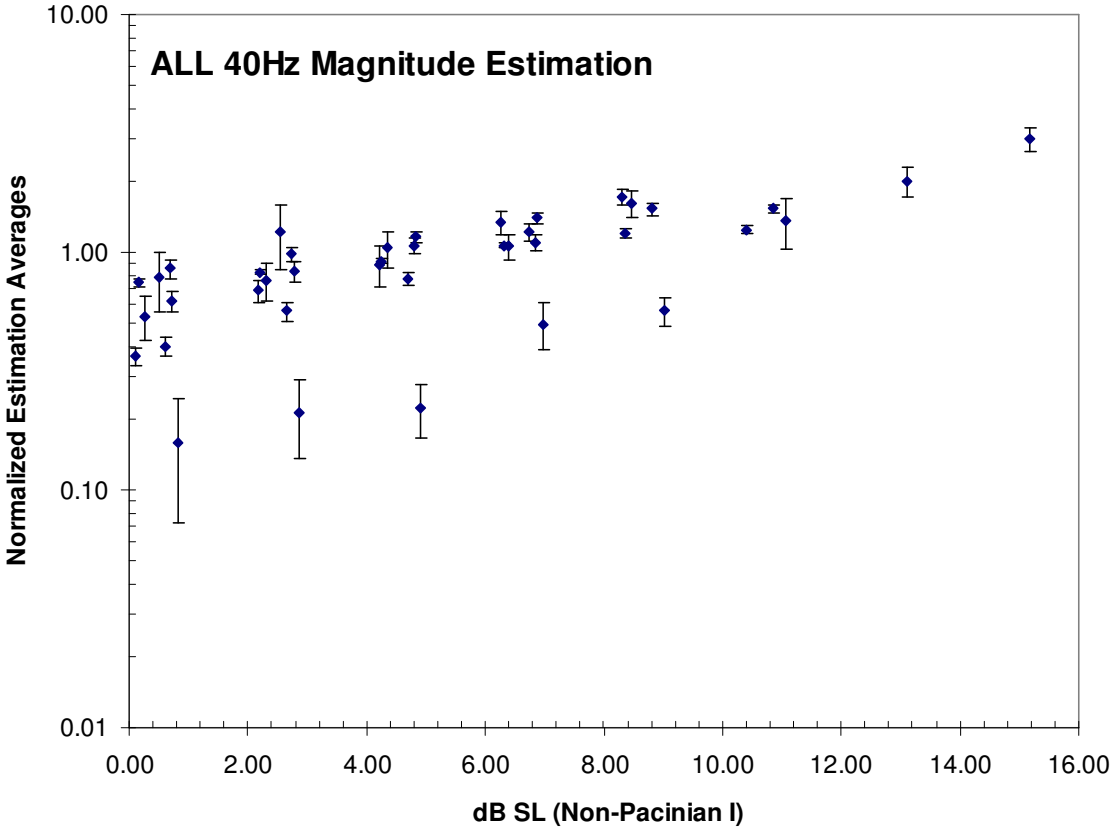

Figure 4.8 Normalized magnitude estimation values for the isolated NP I channel (40 Hz masked) of all subjects. Horizontal axis is the stimulus level referenced to threshold. (Standard error bars are shown on data points).

Table 4.2
Power function exponents, averages, standard deviations and standard errors for three different magnitude estimations.

Subjects	LineLength	40 Hz (NP I) channel Magnitude Estimation	250 Hz (P) channel Magnitude Estimation
S1 (female)	1.478	0.365	0.470
S2 (male)	0.995	1.162	0.813
S3 (female)	1.115	1.900	0.785
S4 (male)	0.864	1.597	0.689
S5 (female)	0.785	1.218	0.676
S6 (male)	0.876	1.886	0.733
S7 (male)	0.923	0.466	0.459
S8 (female)	0.852	1.064	0.842
Average	0.986	1.207	0.683
Stdev	0.223	0.582	0.147
StError	0.079	0.206	0.052

Table 4.3
Statistical comparison of magnitude estimation results for NP I and P channels, and for males and females.

Statistical Comparison	Experimental Condition	Statistical test	Statistical result
40 Hz vs. 250 Hz Magnitude Estimation	40 Hz masked & 250 Hz unmasked	Paired *t*-test	P=0.02 (significant difference)
Men vs. Women 40 Hz Magnitude Estimation	40 Hz masked	Two-sample *t*-test	P=0.76 (no significant difference)
Men vs. Women 250 Hz Magnitude Estimation	250 Hz unmasked	Two-sample *t*-test	P=0.86 (no significant difference)

Table 4.4 shows the statistical comparison of power function exponents obtained from magnitude estimation at 250 Hz with the average literature values. Results obtained in this thesis show statistically significant difference from those of the literature. In this study, stimuli were applied to the fingertip, however, experiments conducted in the literature were done on the thenar emminence of the hand. Thus, this significant difference is expected.

Table 4.4
Statistical comparison of magnitude estimation results for P channel with the literature.

Statistical Comparison	250 Hz magnitude estimation exponents	Location of Applied Stimulus	Statistical test	Statistical Result
Literature [30]	0.89	thenar eminence (9.5mm dia.) right hand	One-sample *t*-test	P=0.0053
Literature [31]	0.94	thenar eminence (7mm dia.) right hand	One-sample *t*-test	P=0.0017
Literature [7]	0.98	thenar eminence (9.5mm dia.) right hand	One-sample *t*-test	P=0.0007
Literature [32]	0.55	thenar eminence (2mm dia.) right hand	One-sample *t*-test	P=0.037

The correlation coefficient between power function exponents of NP I channel and P channel was 0.71. This shows that large exponents obtained for one subject at 40 Hz was also large at 250 Hz.

4.4 Model Simulation Results

After determining the vibrotactile threshold of each subject according to the criterion mentioned in the previous chapter, the change in number of active fibers (see Figure 4.9), total number of spikes (see Figure 4.10) and maximum number of spikes (see Figure 4.11) with respect to the stimulus amplitude (in micrometers) were investigated. In Figure 4.9, Figure 4.10 and Figure 4.11, power functions are plotted and the resulting power function exponents are tabulated in Table 4.5.

In Table 4.6, the experimental power function exponents are compared to those obtained for three model simulations. Power function exponents for model simulation, which used the maximum spike number as the intensity code was significantly different from the experimental exponents. However, the exponents of the other two simulations, which used the number of active fibers and the total number of spikes as intensity codes showed no significant differences with experimental exponents.

As the stimulus amplitude increased normalized number of active fibers (see Figure 4.9), total number of spikes (see Figure 4.10) and maximum number of spikes (see Figure 4.11) of all simulated subjects increased. At the end of this simulation, a power function was fitted to the data points obtained for each simulated subject. At the bottom right-hand corner of each graph, the power functions obtained as the result of this fitting are shown. Goodness of fit values (R^2) are also shown. Power functions gave high goodness of fit values for number of active fibers ($R^2 > 0.98$), total number of spikes ($R^2 > 0.96$) and maximum number of spikes ($R^2 > 0.62$).

Figure 4.12 shows all the data points of the experimental and the three model simulation results together plotted with logarithmic scale. The dark blue dots represent the number of active fibers, the light blue dots represent the total number of spikes and the orange dots represent the maximum number of spikes. However, it is not clear which one of these three models is closer to the experimental data. At this point a new metric was defined to find a relation between experimental results and model results. This new algorithm helps one decide the best model among several different options. According to

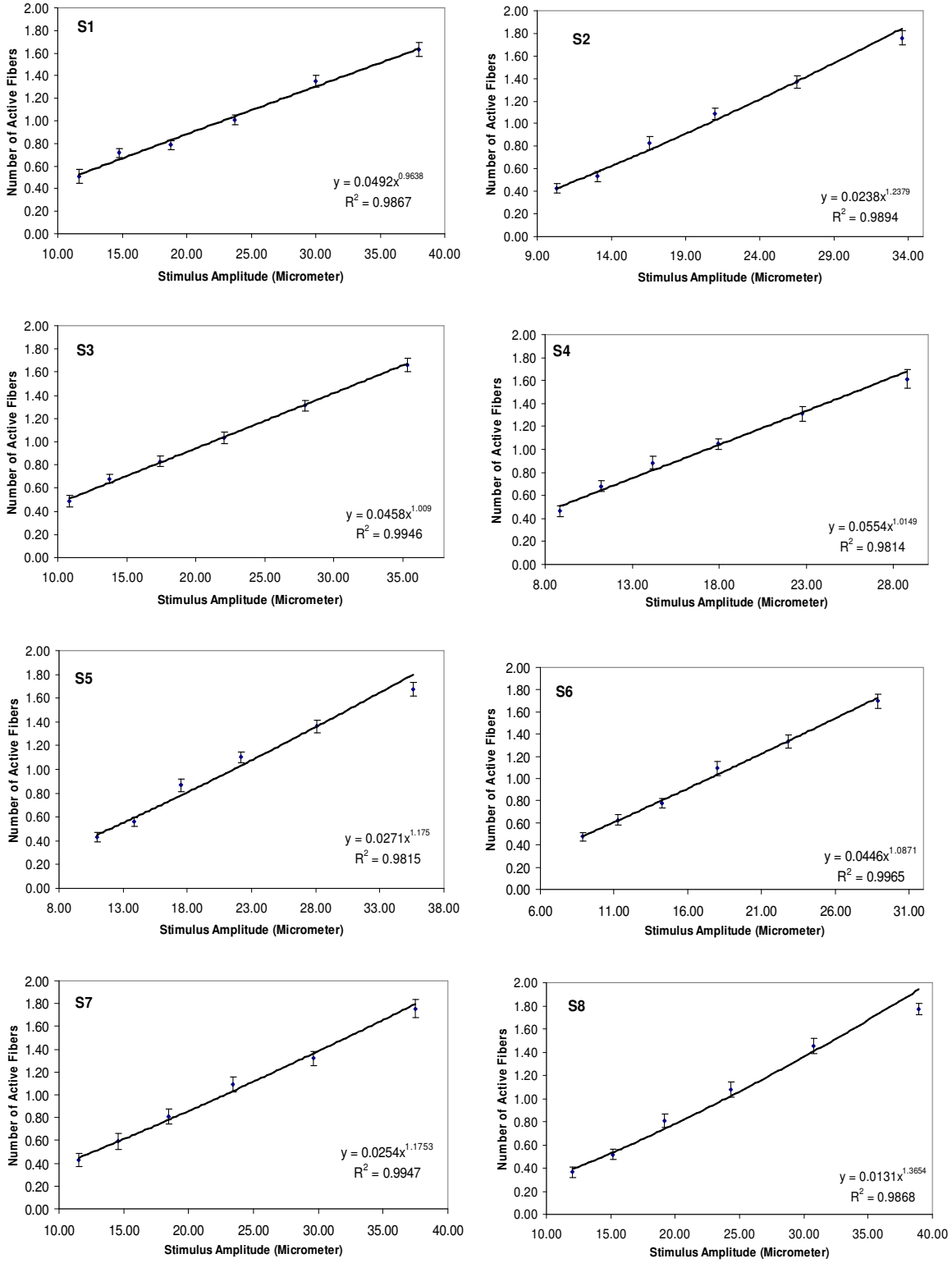

Figure 4.9 Normalized averages of number of active fibers obtained by model simulations. Horizontal axis shows the displacement in micrometers for 40 Hz. The power functions fitted to the data points are also given. (Standard deviation bars are shown on data points).

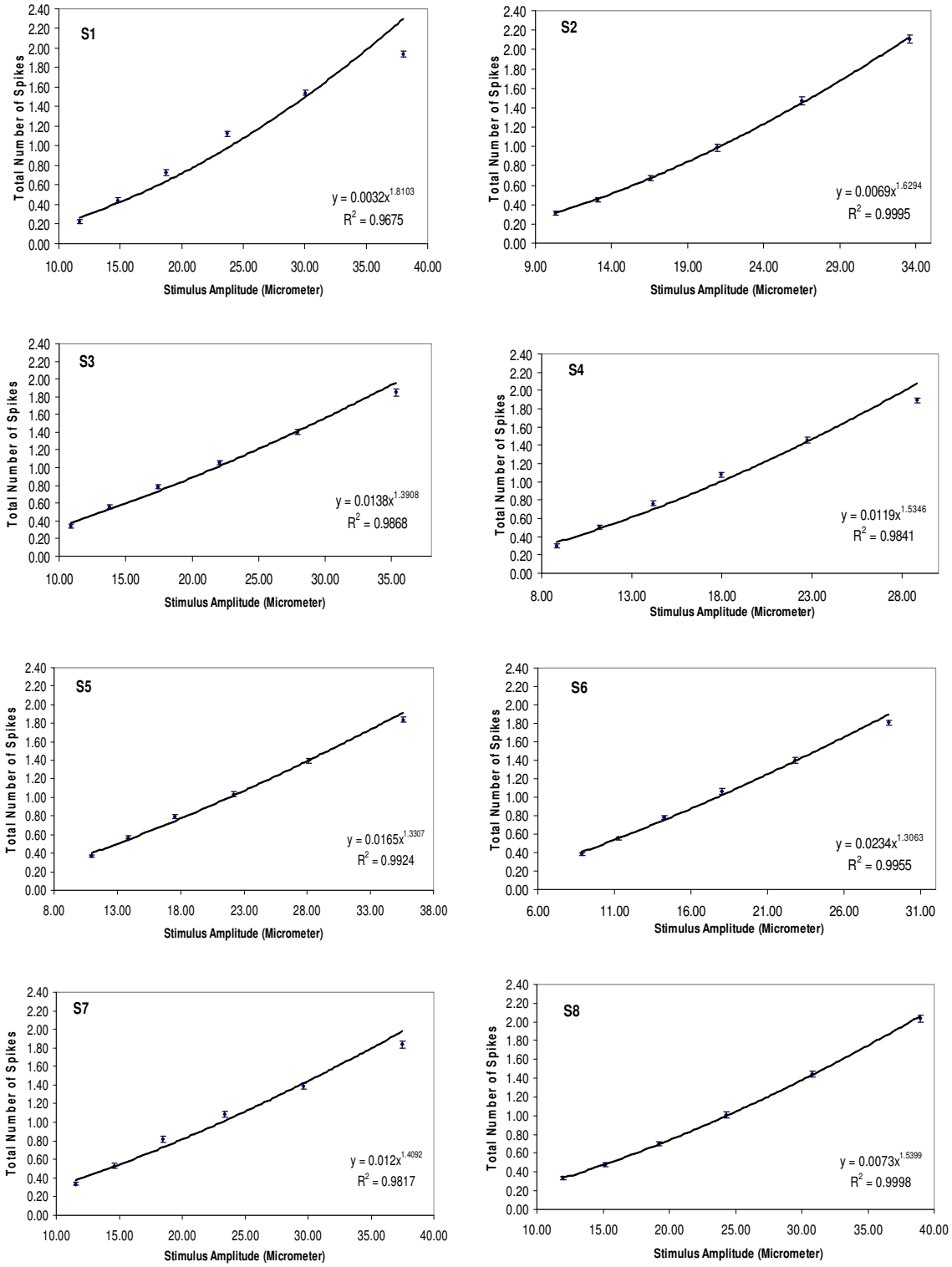

Figure 4.10 Normalized averages of total number of spikes obtained by model stimulations. Horizontal axis shows the displacement in micrometers for 40 Hz. The power functions fitted to the data points are also given. (Standard deviation bars are shown on data points).

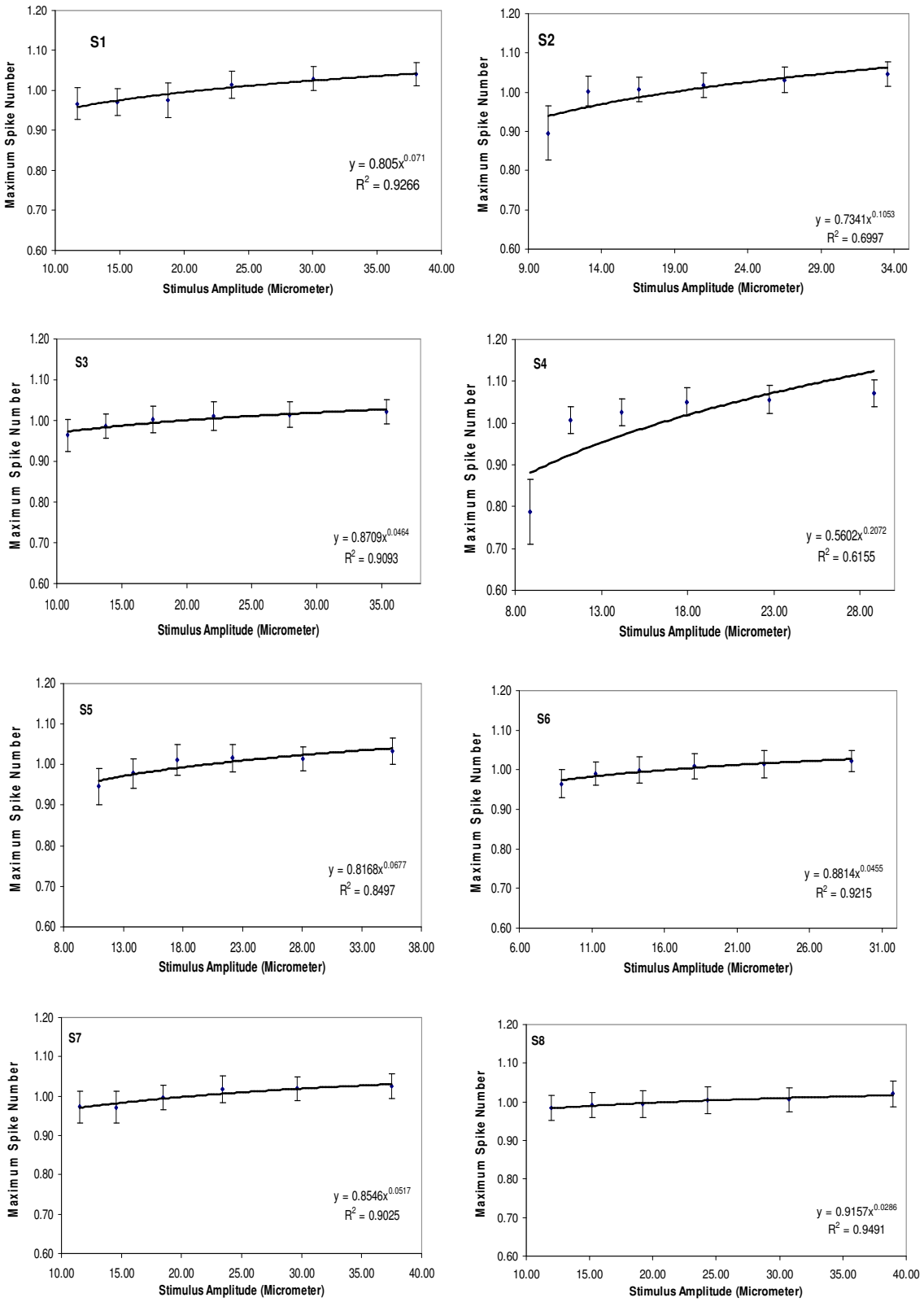

Figure 4.11 Normalized averages of maximum number of spikes obtained by model stimulations. Horizontal axis shows the displacement in micrometers for 40 Hz. The power functions fitted to the data points are also given. (Standard deviation bars are shown on data points).

Table 4.5
Power function exponents, averages, standard deviations and standard errors for experimental magnitude estimations and three different model simulations.

Subjects	40Hz Magnitude Estimation Micrometer	Code: Number of Active Fibers	Code: Total Number of Spikes	Code: Maximum Number of Spikes
S1	0.365	0.964	1.810	0.071
S2	1.162	1.238	1.629	0.105
S3	1.900	1.009	1.391	0.046
S4	1.597	1.015	1.535	0.207
S5	1.218	1.175	1.331	0.068
S6	1.886	1.087	1.306	0.046
S7	0.466	1.175	1.409	0.052
S8	1.064	1.365	1.540	0.029
Average	1.207	1.129	1.494	0.078
Stdev	0.582	0.135	0.170	0.057
StError	0.206	0.048	0.060	0.020

Table 4.6
Statistical comparison of magnitude estimation results for the NP I channel and the model simulations.

Statistical Comparison	Experimental Condition	Statistical test	Statistical result
40 Hz magnitude estimation vs. Model (number of active fibers)	40 Hz masked	Two-sample *t*-test	P=0.719 (no significant difference)
40 Hz magnitude estimation vs. Model (total number of spikes)	40 Hz masked	Two-sample *t*-test	P=0.218 (no significant difference)
40 Hz magnitude estimation vs. Model (max. number of spikes)	40 Hz masked	Two-sample *t*-test	P=0.001 (significant difference)

the algorithm, the closest distance between each data point of the experiment and the model data points was determined and these shortest distances were averaged (refer to Chapter 3. “Methodology”).

The standart error bars of model simulation results cannot be seen in Figure 4.12 since they were very small. The application of the new distance rule required the normalization of both the y-axis and x-axis values. Figure 4.13, shows experimental data and model simulation data (three different intensity codes) with both axes normalized. Table 4.7 shows the results of this new comparison algorithm where intensity code of total number of spikes gave the smallest distance metric.

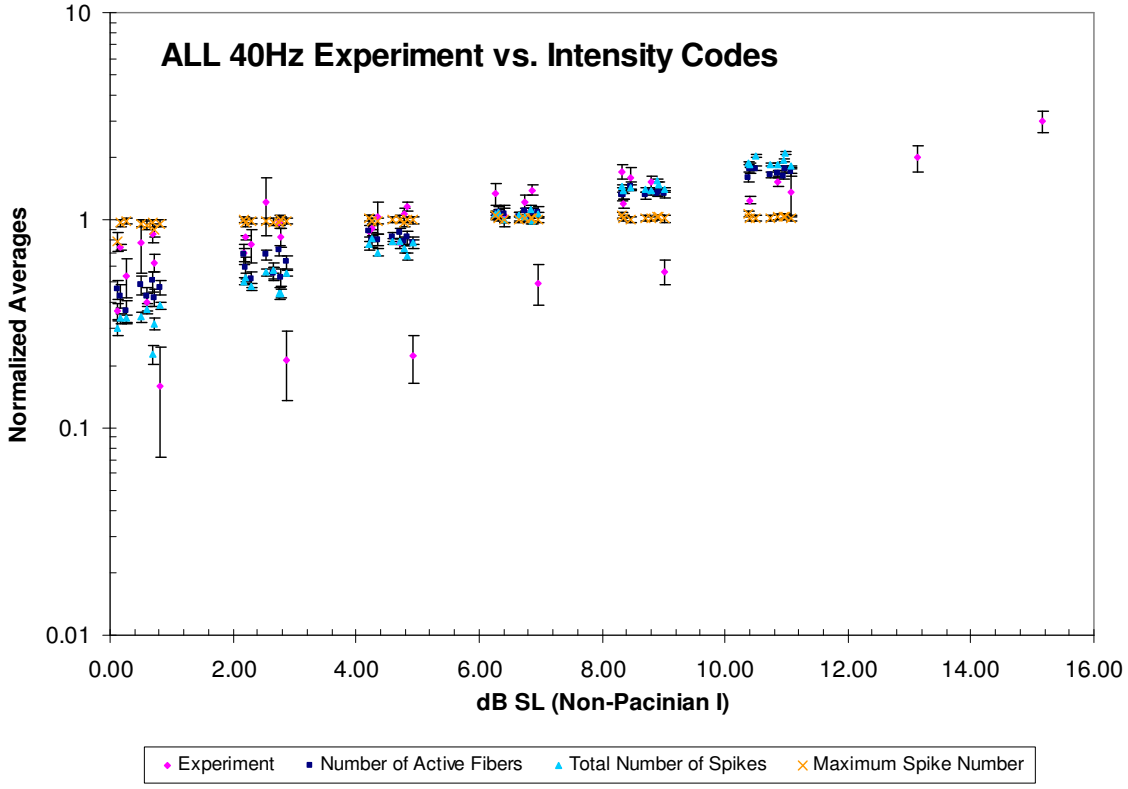

Figure 4.12 Normalized magnitude estimation values for the NP I channel (40 Hz masked) and normalized values of model results. Horizontal axis is the stimulus level referenced to the threshold. (Standard error bars are shown on data points).

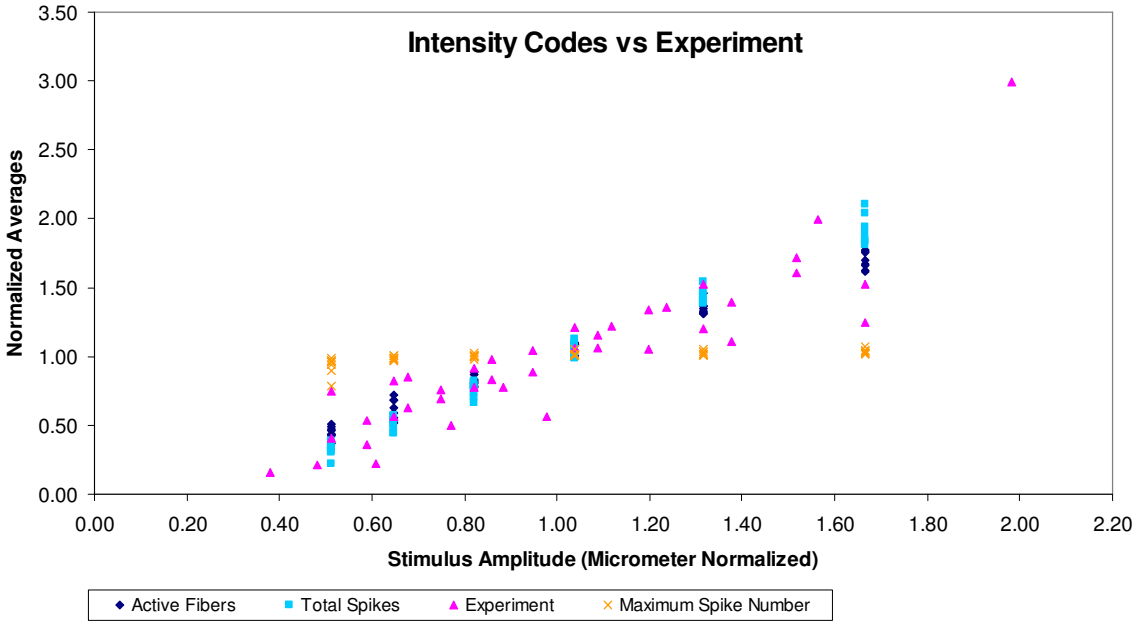

Figure 4.13 Normalized experimental and model simulation results (at 40 Hz). Horizontal axis is the stimulus amplitude in micrometer normalized units. (Standard error bars are not shown on data points).

Table 4.7
Comparison of three intensity codes using a novel distance rule.

Comparison	Distance metric (shortest distances)
Model (number of active fibers) vs. Experiment	0.035
Model (total number of spikes) vs. Experiment	0.023

Table 4.8 shows the goodness of fit values obtained as a result of fitting power functions and logarithmic functions to the experimental and model simulation results. Shaded regions show which one of the two goodness of fit values is closer to the value of "1". According to Table 4.8, goodness of fit values obtained for the experiments by fitting logarithmic functions were generally greater compared to those obtained by fitting power functions. In contrast, goodness of fit values obtained for the model simulations by fitting logarithmic functions were generally smaller compared to those obtained by fitting power functions.

Table 4.8
Goodness of fit values for logarithmic and power function fits.

	R^2 (Active Fibers)		R^2 (40Hz)		R^2 (Total Spikes)		R^2 (250Hz)	
	Logarithmic	Power	Logarithmic	Power	Logarithmic	Power	Logarithmic	Power
S1	0.963	0.987	0.947	0.933	0.987	0.967	0.906	0.880
S2	0.980	0.989	0.992	0.989	0.934	0.999	0.989	0.988
S3	0.975	0.995	1.000	1.000	0.979	0.987	0.918	0.898
S4	0.990	0.981	0.986	0.970	0.982	0.984	0.853	0.879
S5	0.990	0.982	0.955	0.950	0.974	0.992	0.960	0.879
S6	0.975	0.996	0.828	0.968	0.978	0.995	0.728	0.678
S7	0.976	0.995	0.985	0.984	0.985	0.982	0.981	0.997
S8	0.986	0.987	0.919	0.948	0.944	0.999	0.962	0.946

5. DISCUSSION

Magnitude estimation experiments performed in this thesis did not find any solution to a particular disease or tactile disorder; however, it was useful to study the origins of power law. As described in the early chapters, one of the fundamental issues in psychophysics concerns the form of the psychophysical law and the discovery of a simple equation. The form of relationship (the power law) between sensation magnitude and stimulus intensity proposed by S. S. Stevens (1958) is still the center of many experimental [2, 4-7, 22, 29, 30] and modeling [8, 17, 27] studies. Therefore, the results of this thesis are important because of its experimental contribution to psychophysical studies regarding the power law and magnitude estimation, and contribution in terms of validating the previous modeling studies.

5.1 Theshold and Masking Experiments

Threshold and masking experiments performed in this study were important for magnitude estimation experiments since the latter is dependent on the outcomes of the first two types of experiments. Measured values and the literature values (in terms of threshold and masking experiments) had statistically no significant difference which suggests that the current results are consistent with previous data. In psychophysical studies, subject groups are usually small. Therefore, as more experiments are performed and their results are validated with the literature, the pool of such studies becomes larger. As a result, with a larger pool of experimental results, better generalizations (modeling studies) can be done.

Figure 4.3 shows that as the stimulus is increased the shift in threshold increases, and this can be represented with a linear fit. Since more complicated models were not needed for the purpose of this study linear fit is adequate. The reason of such psychophysical threshold shifts could be a central network phenomenon. The refractory period of tactile fibers can be as small as 1-2 ms, however, larger recovery periods might be expected in the central network. The signals from the spinal cord travel directly to the

dorsal column nuclei of the brain stem and synapses are only available from there on [9]. Therefore, due to the chemical effects, signals that are transmitted by the neurotransmitters have a longer effect, probably causing the weaker stimuli to be suppressed. This means that after masking stimuli, stronger test stimuli are needed so that the higher order neurons can differentiate between the two signals. Psychophysically, this indicates an upward shift in the threshold. In the literature it was demonstrated that as the time delay between a masking stimulus and a test stimulus is increased there is a decay in the effectiveness of the masking stimulus. After a certain time delay (100-200 ms for stimulating the P channel), this decay reaches a plateau therefore, in this study, a time delay (150 ms) in such a range was selected. Due to the residual masking effect (after the masking stimulus is terminated), some of the higher order neurons probably do not recover from their active state and thus cannot respond to the proceeding test stimuli at 250 Hz, therefore a shift in the threshold is observed. If the masking stimulus is increased even more, the residual effect increases as well [18].

The increase in the thresholds at 40 Hz after inducing masking (see Figure 4.4) shows that at 40 Hz the most sensitive channel is not the NP I channel but the P channel. Therefore, by assuming that masking at 250 Hz would elevate the threshold by a similar amount at 40 Hz, threshold shift at 250 Hz was added to that of 40 Hz to find the dynamic range of the NP I channel. As can be seen from Figure 4.4, some of these ranges can be quite narrow. That was why, for some of the subjects, less data points were collected. The dynamic range for each subject could be increased by using higher intensity masking functions, however, there is a limit to increasing the stimulus amplitude (<250 micrometers). Beyond this limit decoupling of the contactor from the skin would occur [21]. Another alternative would be to increase the duration of masking stimulus. As the duration of the masking stimulus is increased, the temporal effect of masking increases therefore, the threshold shifts obtained at the end of masking would be higher [33]. Higher threshold shift would increase the dynamic range. However, for the experiments performed in this study, masking stimuli durations were 1 sec. Increasing this duration would increase the masking effect but would also increase the experiment time. Shorter durations would yield narrower dynamic ranges, thus during magnitude estimation experiments inadequate amount of data points would be collected.

According to Figure 4.3, the goodness of fit values of the linear trend lines are quite good (R^2>0.84) except for three subjects (S2, S3 and S6). Worse goodness of fit values compared to other subjects are due to at least one data point which shows higher threshold shift than expected. All four data points from one subject were not taken on the same day, therefore, this difference might be due to the subject's variablity at that time.

5.2 Magnitude Estimation Experiments

The first hypothesis of this study claimed that magnitude estimation would yield power functions. All the experimental results and model simulation results were successfully expressed with the power law. Different power function exponents suggested that the relation between the sensation magnitude and stimulus intensity was different for each person. Similar fits using logarithmic functions were done and in case of the experiments, goodness of fit values for these logarithmic functions were generally better compared to those of the power functions. However, the opposite was true in case of model simulations. The aim in this thesis was to see whether if power function was a good fit for the experiments and model simulations but not a comparison with the logarithmic fits. However, the difference between the goodness of fit of power functions and logarithmic functions for the model simulations and the experiments were comparably small, therefore, my first hypothesis is verified.

The normalization procedure applied on magnitude estimation data allows the experimenter to compare the responses of different subjects. This type of manipulation eliminates the subjective nature of magnitude estimation up to a certain extent. In the experiment, the aim was to be able to compare different data sets rather than obtaining a single standard for every data set. An alternative approach could be the magnitude production method [1]. In that case, subject is presented with the numerical value of a sensory magnitude and then he/she is required to adjust the stimulus producing that sensation. Using this method could be valuable to test the validity of magnitude estimation experiments performed in this thesis. Using both methods in the experiments would probably eliminate any systematic errors inherent in these methods. One of the inherent errors stated in the literature is the regression bias [1]. According to the regression bias, the

subjects are conservative in their judgments which mean that they are reluctant to make extremely low or extremely high judgments even though they may be correct by their perceptions. That was probably why subjects used in this study never gave numbers higher than 100 or smaller than 0.01.

Magnitude estimation at 250 Hz by the P channel was compared to magnitude estimation at 40 Hz by the NP I channel. The hypothesis that magnitude estimation values can be expressed by power functions was validated. The power functions fit well to the magnitude estimation data shown in Figure 4.5 ($R^2 > 0.67$) and in Figure 4.7 ($R^2 > 0.93$). The power exponents at 40 Hz are larger than those at 250 Hz (only one exception) which means that magnitude estimation at 40 Hz results in steeper power functions. This difference was also shown statistically by a paired *t*-test (see Table 4.3). Such difference at these two frequencies might be because of more neurons being recruited at 40 Hz in the NP I channel than at 250 Hz in the P channel which also suggests that the two information channels operate differently at those frequencies.

Figures 4.6 and 4.8 show that all the experimental data, when plotted on a logarithmic scale, follow a linear trend. This means that on a linear scale the data points follow the power law.

There are no statistical differences between male and female subjects in terms of power exponents. The importance of such a discovery is that generalizations can be done disregarding the gender effects. Model simulations do not have to account differently for male and female scenarios. Unfortunately, statistical comparison of male and female exponents with the literature was not done because such discrimination was not found in the psychophysical literature. However, there was one study where magnitude estimation experiments were performed on the tongue and male-female difference was investigated (Fucci et. al. 1990). According to this study, men and women have tactile sensory systems that operate similarly at both threshold and suprathreshold levels of stimulation. However, they used consistently different numerical responses to suprathreshold stimuli. This suggests that there is difference between male and female magnitude estimation, however it does not mean that their power function exponents will show this difference. Also, one cannot generalize this consequence to an experiment done on the fingertip.

The experiment and model simulation findings suggest that as the power exponents become larger (steeper lines on logarithmic scale) the power function coefficients become smaller. The direct comparison of sensation magnitude and stimulus intensity is given by the power exponents however, one can also say by comparing the power function coefficients that the slope of such relation has increased or decreased. Unfortunately, power function coefficients do not reveal much information about the behavior of sensation magnitude when stimulus intensity is increased.

5.3 Model Simulations

When the contactor surround is not used, highly sensitive fibers located away from the contactor can be activated. The presence of a contactor surround facilitates masking and increases the threshold at higher frequencies whereas at lower frequencies thresholds decrease [34, 35]. The presence of the contactor surround also makes the modelling difficult since it introduces an additional edge on the skin. This factor must be included in the model as well. For 40 Hz-stimulation, presence of a surround did not have any effect on threshold [27]. However, the model simulated here does not include the contactor surround since physiological data used to create the model were obtained without a surround. Therefore in the experiments, also no contactor surround was used.

The power function fits were applied with normalized averages on y-axis and stimulus amplitudes in micrometers on x-axis. According to these fitted curves, there are values below the sensation thresholds. This seems like a contradiction, because subjects cannot give magnitude estimates below threshold. Nevertheless, there can be neural activation below the threshold. Therefore, the fits are still meaningful.

Statistically significant difference between the experimental power exponents and the simulation exponents obtained with the maximum spike number as the intensity code suggests that the maximum spike number is not used for magnitude estimation in the tactile system. The data points for the total number of spikes lie closer to the experimental data points.

The second hypothesis of this study was that the number of active tactile fibers is the intensity code used for magnitude estimation and that this relation is in terms of power law. Statistical analyses suggest that number of active fibers and total number of spikes can both be the intensity code used for magnitude estimation and that their relation to the experimental results is in terms of power law. However, according to the new distance rule, total number of spikes generated by the active rapidly-adapting fibers simulates the experimental data better. An active fiber produces at least one spike which means that it may also generate more spikes; therefore the increase in the total number of spikes does not have a linear relation with the increase in the number of active fibers [17]. Thus, these two intensity codes are expected to represent the magnitude estimation results in a similar way but not in the same way. That is why, in Figure 4.13, simulation results of these two intensity codes were very close to each other and that their distance metrics were on the same order of magnitude.

Electrical signal transduction is dependent on the generation of spikes. The total number of spikes represents the total activity going on in the tactile system by giving precise information on the number of spikes that are generated. However, the number of active fibers yields indirect information about an increase in the number of spikes. Depending on the distance metric and the above discussion, the total number of spikes is the more appropriate intensity code for representing the experimental data.

6. FUTURE CONSIDERATIONS

To be able to understand the tactile system better and develop systems that better imitate human tactile sensation, the perception of stimulus magnitude should be better understood (i.e. how the information from different channels are integrated in the higher brain regions). The experiments presented here provide a basis for the mathematical models developed and that are yet to be developed.

Sensory Integration Dysfunction is a neurological disorder causing difficulties with processing information from the five classic senses (vision, auditory, touch, olfaction, and taste), the sense of movement (vestibular system), and/or the positional sense (proprioception) [36]. Sensory information is sensed normally, but perceived abnormally. Sensory integration dysfunction can be a disorder on its own, but it can also be a characteristic of other neurological conditions, such as autism. Indicators of autism include oversensitivity or under reactivity to touch [37]. This study can be extended by experimenting on autistic children and see how they would respond to magnitude estimation task. The significance of such studies would be to find more about the neuropathology of autism regarding brain regions with sensory input and for basic processing of tactile information [38]. Eventually, comparison can be made with normal children. In further studies, by doing experiments on different age groups and on stroke patients who are reported to have reduction in sensory or vibratory sensation [39], more issues on tactile psychophysics can be investigated and by simultaneously acquiring brain EEG signals, higher level of psychophysical investigations can be carried out.

All the subjects used in the experiments were right-handed and their left middle fingers were stimulated. Same procedures may be done on right middle fingers of the same subjects. If statistically significant differences were to be found, then it would be suspected that information processing channels should be different for the right and left hands of the same person.

Today's technology is capable of making hand transplants to people who had lost their hands in accidents [40]. With increasing studies, as the one in this thesis, and with the advancement of technology, artifical human hands with mechanoreceptors can be manufactured.

APPENDIX A. MATLAB CODES

A.1 Matlab Code for Magnitude Estimation Experiment

```
%girdiler  callback function to enter the inputs
uyar=input('Uyarilar neler? (Matrix olarak yaz -- [] seklinde)');
meze=size(uyar);
uyar=ones(10,1)*uyar;
hey=uyar(randperm(10*meze(2)));
rast=reshape(hey,10,[]);
%magnitude_estim  callback function to run experiment
h6 = hgload('magni_es.fig');
handles6 = guihandles(h6);
cla;
reset_stim;
temp = size(exp_data);
trial_no = temp(1);
if trial_no > 0
   ch1wf1att = exp_data(trial_no,1);
   ch1wf2att = exp_data(trial_no,2);
   set(handles6.text21,'String',num2str(trial_no));
   set(handles6.text5,'String',num2str(ch1wf1att));
   set(handles6.text6,'String',num2str(ch1wf2att));
end
```

A.2 Matlab Code to Start the Experiment

```
%START_EXP   callback function to start experiment
% use only for magnitude estimation with forward-masking
% wf1: masking stimulus, att.: wf1_attstart1
% wf2: test stimulus, att.: wf2_attstart1
wf1;
```

```
wf2;
wfdelta1 = 1.085; % time between wf1 and wf2
wfdelta2 = 0.675; % time after wf2
exp_data = [];
plot_magni;
say=1;
stopix = 0;
trial_no = 0;
att1=str2num(get(handles6.edit13,'String'));
sayac=1;
  while ~stopix,
    switch sayac
        case 1
          set(handles6.edit1,'BackgroundColor','cyan');
          set(handles6.edit1,'String',rast(say,1));
          att2=str2num(get(handles6.edit1,'String'));
        case 2
          set(handles6.edit2,'BackgroundColor','cyan');
          set(handles6.edit2,'String',rast(say,2));
          att2=str2num(get(handles6.edit2,'String'));
        case 3
          set(handles6.edit3,'BackgroundColor','cyan');
          set(handles6.edit3,'String',rast(say,3));
          att2=str2num(get(handles6.edit3,'String'));
        case 4
          set(handles6.edit4,'BackgroundColor','cyan');
          set(handles6.edit4,'String',rast(say,4));
          att2=str2num(get(handles6.edit4,'String'));
        case 5
          set(handles6.edit5,'BackgroundColor','cyan');
          set(handles6.edit5,'String',rast(say,5));
          att2=str2num(get(handles6.edit5,'String'));
        case 6
          set(handles6.edit6,'BackgroundColor','cyan');
          set(handles6.edit6,'String',rast(say,6));
          att2=str2num(get(handles6.edit6,'String'));
```

```
    case 7
      set(handles6.edit14,'BackgroundColor','cyan');
      set(handles6.edit14,'String',rast(say,7));
      att2=str2num(get(handles6.edit14,'String'));
    case 8
      set(handles6.edit15,'BackgroundColor','cyan');
      set(handles6.edit15,'String',rast(say,8));
      att2=str2num(get(handles6.edit15,'String'));
    case 9
      set(handles6.edit22,'BackgroundColor','cyan');
      set(handles6.edit22,'String',rast(say,9));
      att2=str2num(get(handles6.edit22,'String'));
    case 10
      set(handles6.edit23,'BackgroundColor','cyan');
      set(handles6.edit23,'String',rast(say,10));
      att2=str2num(get(handles6.edit23,'String'));
    case 11
      set(handles6.edit24,'BackgroundColor','cyan');
      set(handles6.edit24,'String',rast(say,11));
      att2=str2num(get(handles6.edit24,'String'));
  end
  set(handles6.text3,'String','RUNNING...');
  set(handles6.text3,'BackgroundColor','cyan');
  trial_no = trial_no + 1;
  set(handles6.text21,'String',num2str(trial_no));
  set(handles6.text5,'String',num2str(att1));
  set(handles6.text6,'String',num2str(att2));
% run equipment
invoke(PA5,'ConnectPA5','USB',1);
      putvalue(dio.line(9),1);
      invoke(PA5,'SetAtten',att1);
      putdata(ao,wf_1');
      start(ao);
      pause(wfdelta1);
      stop(ao);
      invoke(PA5,'SetAtten',att2);
```

```
      putdata(ao,wf_2');
      start(ao);
      pause(wfdelta2);
      stop(ao);
      putvalue(dio.line(9),0);
uiwait
switch sayac
    case 1
       set(handles6.edit1,'BackgroundColor','white');
      cevap=str2num(get(handles6.edit7,'String'));
    case 2
       set(handles6.edit2,'BackgroundColor','white');
      cevap=str2num(get(handles6.edit8,'String'));
    case 3
       set(handles6.edit3,'BackgroundColor','white');
      cevap=str2num(get(handles6.edit9,'String'));
    case 4
       set(handles6.edit4,'BackgroundColor','white');
      cevap=str2num(get(handles6.edit10,'String'));
    case 5
       set(handles6.edit5,'BackgroundColor','white');
      cevap=str2num(get(handles6.edit11,'String'));
    case 6
       set(handles6.edit6,'BackgroundColor','white');
      cevap=str2num(get(handles6.edit12,'String'));
    case 7
       set(handles6.edit14,'BackgroundColor','white');
      cevap=str2num(get(handles6.edit18,'String'));
    case 8
       set(handles6.edit15,'BackgroundColor','white');
      cevap=str2num(get(handles6.edit19,'String'));
    case 9
       set(handles6.edit22,'BackgroundColor','white');
      cevap=str2num(get(handles6.edit25,'String'));
    case 10
       set(handles6.edit23,'BackgroundColor','white');
```

```
        cevap=str2num(get(handles6.edit26,'String'));
      case 11
        set(handles6.edit24,'BackgroundColor','white');
        cevap=str2num(get(handles6.edit27,'String'));
  end
  exp_data = [exp_data; [att1 att2 cevap]];
  sayac=sayac+1;
 plot_magni;
 if sayac>meze(2)
    sayac=1;
    say=say+1;
 end
 if say>10
    stopix=1;
 end
end
 set(handles6.text3,'String','STOPPED.');
 set(handles6.text3,'BackgroundColor','white');
```

A.3 Matlab Code for Distance Metric

```
% Model vs. Experiment  (distance metric)
experiment=[1.38 1.10;1.09 1.07;0.86 0.98;0.68 0.85;1.38 1.39;1.09 1.16;0.86 0.83;0.68 0.62;1.12
1.22;0.88  0.78;1.52  1.71;1.20  1.34;0.95  0.89;0.75  0.69;0.59  0.36;1.67  1.52;1.32  1.52;1.04
1.21;0.82  0.77;0.65  0.57;0.51  0.40;1.98  3.00;1.56  1.99;1.24  1.36;0.98  0.56;0.77  0.50;0.61
0.22;0.48  0.21;0.38  0.16;1.67  1.25;1.32  1.20;1.04  1.06;0.82  0.92;0.65  0.83;0.51  0.74;1.52
1.60;1.20 1.06;0.95 1.04;0.75 0.76;0.59 0.54];

model1=[0.51  0.51;0.65  0.72;0.82  0.79;1.04  1.01;1.32  1.35;1.67  1.63;0.51  0.42;0.65  0.53;0.82
0.82;1.04  1.09;1.32  1.37;1.67  1.76;0.51  0.49;0.65  0.68;0.82  0.83;1.04  1.03;1.32  1.31;1.67
1.66;0.51  0.46;0.65  0.68;0.82  0.89;1.04  1.05;1.32  1.31;1.67  1.61;0.51  0.43;0.65  0.56;0.82
0.87;1.04  1.10;1.32  1.36;1.67  1.68;  0.51  0.47;0.65  0.63;0.82  0.78;1.04  1.09;1.32  1.33;1.67
1.70;0.51  0.43;0.65  0.59;0.82  0.81;1.04  1.09;1.32  1.32;1.67  1.76;0.51  0.37;0.65  0.52;0.82
0.81;1.04 1.08;1.32 1.46;1.66 1.77];
```

```
model2=[0.51 0.22;0.65 0.44;0.82 0.73;1.04 1.12;1.32 1.54;1.67 1.94;0.51 0.32;0.65 0.45;0.82
0.67;1.04 0.99;1.32 1.47;1.67 2.11;0.51 0.34;0.65 0.56;0.82 0.79;1.04 1.06;1.32 1.40;1.67
1.85;0.51 0.30;0.65 0.51;0.82 0.77;1.04 1.08;1.32 1.45;1.67 1.89;0.51 0.37;0.65 0.57;0.82
0.79;1.04 1.04;1.32 1.40;1.67 1.84;0.51 0.39;0.65 0.56;0.82 0.78;1.04 1.06;1.32 1.40;1.67
1.81;0.51 0.34;0.65 0.53;0.82 0.82;1.04 1.09;1.32 1.39;1.67 1.84;0.51 0.33;0.65 0.48;0.82
0.70;1.04 1.01;1.32 1.44;1.66 2.04];

model3=[0.51 0.966;0.65 0.971;0.82 0.975;1.04 1.014;1.32 1.030;1.67 1.041;0.51 0.895;0.65
1.002;0.82 1.006;1.04 1.017;1.32 1.031;1.67 1.046;0.51 0.964;0.65 0.986;0.82 1.002;1.04
1.009;1.32 1.014;1.67 1.022;0.51 0.787;0.65 1.006;0.82 1.026;1.04 1.050;1.32 1.056;1.67
1.072;0.51 0.946;0.65 0.978;0.82 1.010;1.04 1.016;1.32 1.015;1.67 1.033;0.51 0.964;0.65
0.990;0.82 0.998;1.04 1.008;1.32 1.014;1.67 1.023;0.51 0.971;0.65 0.971;0.82 0.996;1.04
1.016;1.32 1.019;1.67 1.024;0.51 0.983;0.65 0.991;0.82 0.993;1.04 1.004;1.32 1.005;1.66 1.020];

tumdata=[experiment;model1;model2;model3];
mesafe=pdist(tumdata);
mesafesonuc=squareform(mesafe);
for i=1:40;
enkisamesafe(i)=min(mesafesonuc(i,41:88)); %experiment vs model1
enkisamesafe2(i)=min(mesafesonuc(i,89:136)); %experiment vs model2
enkisamesafe3(i)=min(mesafesonuc(i,137:184)); %experiment vs model3
end
mexpm1=mean(enkisamesafe);
mexpm2=mean(enkisamesafe2);
mexpm3=mean(enkisamesafe3);
stexpm1=std(enkisamesafe);
stexpm2=std(enkisamesafe2);
stexpm3=std(enkisamesafe3);

for i=41:88;
enkisamesafe4(i)=min(mesafesonuc(i,1:40)); %model1 vs experiment
end
mexpm4=mean(enkisamesafe4);
stexpm4=std(enkisamesafe4);
for i=89:136;
```

```
enkisamesafe5(i)=min(mesafesonuc(i,1:40)); %model2 vs experiment
end
mexpm5=mean(enkisamesafe5);
stexpm5=std(enkisamesafe5);
for i=137:184;
enkisamesafe6(i)=min(mesafesonuc(i,1:40)); %model3 vs experiment
end
mexpm6=mean(enkisamesafe6);
stexpm6=std(enkisamesafe6);
sonuclar=[mexpm1 stexpm1; mexpm4 stexpm4; mexpm2 stexpm2; mexpm5 stexpm5; mexpm3 stexpm3;
mexpm6 stexpm6];
```

REFERENCES

1. Gescheider, G. A., *Psychophysics: The Fundamentals*, 3rd edition, LEA, New Jersey, 1997.

2. Fucci, D., L. Petrosino, and S. Wagner, "Vibrotactile threshold shift during magnitude-estimation scaling on the hand: Effects on magnitude-estimation responses and scaling behavior," *Perceptual & Motor Skills*, Vol. 69, pp. 187-194, 1989.

3. Marks, L.E., *Sensory processes: the new psychophysics,* Academic Press, New York, 1974.

4. Harris, D., D. Fucci, L. Petrosino, and D. Wallace, "Instrumentation for magnitude estimation and cross-modality matching of auditory and lingual vibrotactile sensations," *Rev. Sci. Instrum.*, Vol. 57(9), pp. 2343-2347, September 1986.

5. Pare, M., H. Carnahan, and A. M. Smith, "Magnitude estimation of tangential force applied to the fingerpad," *Exp. Brain Research*, Vol. 142, pp. 342-348, 2002.

6. Verrillo, R. T., S. J. Bolanowski, and F. McGlone, "Subjective magnitude of tactile roughness," *Somatosensory & Motor Research*, Vol. 16(4), pp. 352-360, 1999.

7. Verrillo, R. T., and S. J. Bolanowski, "Effects of temperature on the subjective magnitude of vibration," *Somatosensory & Motor Research*, Vol. 20(2), pp. 133-137, June 2003.

8. Güçlü, B., and S. J. Bolanowski, "Modeling Population Responses of Rapidly-Adapting Mechanoreceptive Fibers," *J. Computational Neuroscience*, Vol. 12, pp. 201-218, 2002.

9. Bolanowski, S. J., "Somatosensory Coding", In *Signals and Perception: The Fundamentals of Human Sensation,* D. Roberts (Ed.), The Open University, Palgrave Macmillan, 2002.

10. Gray, J., P&G Skin Care Research Center , "*The World of Skin Care*," 1997. Available: http://www.pg.com/science/skincare/Skin_tws_9.htm.

11. Öztek, Ç., "Measurement of vibrotactile thresholds of normal children," Master's thesis, Boğaziçi University, Istanbul, Turkey, 2006.

12. Hamann, W., "Mammalian cutaneous mechanoreceptors," *Prog. Biophys. Molec. Biol.*, Vol. 64(1), pp. 81-104, 1995.

13. Snodgrass, J., "Psychophysics," In Scharf, B. (Ed.) *Experimental Sensory Psychology*, pp. 17-67, 1975.

14. Gescheider, G. A., S. J. Bolanowski, J.V. Pope, and R. T. Verrillo, "A four-channel analysis of the tactile sensitivity of the fingertip: frequency selectivity, spatial summation, and temporal summation," *Soma. & Mot. Res.,* Vol. 19(2), pp. 114-124, 2002.

15. Gescheider, G. A., S. J. Bolanowski, and R. T. Verrillo, "Some characteristics of tactile channels," *Behavioural Brain Research,* Vol. 148, pp. 35-40, 2004.

16. Greenspan, J. D., and S. J. Bolanowski, "The psychophysics of tactile perception and its peripheral physiological basis," In *Handbook of Perception and Cognition 7: Pain and Touch,* L. Kruger (Ed.), San Diego: Academic Press, 1996.

17. Güçlü, B., and S. J. Bolanowski, "Vibrotactile thresholds of the Non-Pacinian I channel: II. Predicting the effects of contactor location on the phalanx," *Somatosensory & Motor Research*, Vol. 22(1/2), pp. 57-68, March/June 2005.

18. Makous, J. C., G. A. Gescheider, and S. J. Bolanowski, "Decay in the effect of vibrotactile masking," *Journal of the Acoustical Society of America*, Vol. 99(2), pp. 1124-1129, February 1996.

19. Makous, J. C., G. A. Gescheider, and S. J. Bolanowski, "The effects of static indentation on vibrotactile threshold," *Journal of the Acoustical Society of America,* Vol. 99*,* pp. 3149-3153, 1996.

20. Zwislocki, J. J., and E. M. Relkin, "On a psychophysical transformed-rule up and down method converging on a 75% level of correct responses," *PNAS*, Vol. 98, pp. 4811-4814, 2001.

21. Cohen, J. C., J. C. Makous, and S. J. Bolanowski, "Under which conditions do the skin and probe decouple during sinusoidal vibrations?," *Experimental Brain Research*, Vol. 129, pp. 211-217, 1999.

22. Bolanowski, S. J., and G. A. Gescheider, *Ratio Scaling of Psychological Magnitude: In Honor of the Memory of S.S. Stevens,* L. A. Erlbaum, Hillsdale, New Jersey, 1991.

23. Grinstead, C. M., and J. L. Snell, *Introduction to Probability*, Second Revised Edition, Dartmouth College, Hannover, 1997.

24. Breiman, L., *Probability,* published by Addison-Wesley, 1968, reprinted by Society for Industrial and Applied Mathematics, 1992.

25. Markov, A. A., "Extension of the limit theorems of probability theory to a sum of variables connected in a chain," reprinted in Appendix B of: R. Howard. *Dynamic Probabilistic Systems, volume 1: Markov Chains*. John Wiley and Sons, 1971.

26. Güçlü, B., and S. J. Bolanowski, "Tristate Markov Model for the Firing Statistics of Rapidly-Adapting Mechanoreceptive Fibers," *J. Computational Neuroscience*, Vol. 17, pp. 107-126, 2004.

27. Güçlü, B., and S. J. Bolanowski, "Vibrotactile thresholds of the Non-Pacinian I channel: I. Methodological issues," *Somatosensory & Motor Research*, Vol. 22(1/2), pp. 49-56, March/June 2005.

28. Kalkancı, Ö., and B. Güçlü, *Insanlarda Pacini (P) dokunma kanalının maskelenmesi (Masking of the Pacinian (P) Tactile Channel in Humans)*, BİYOMUT, Boğaziçi University, Istanbul, 2005.

29. Zwislocki, J. J. and D. A. Goodman, "Absolute scaling of sensory magnitudes: A validation," *Perception & Psychophysics,* Vol. 28 (1), pp. 28-38, 1980.

30. Verillo, R. T., A. J. Fraioli, and R. L. Smith, "Sensation magnitude of vibrotactile stimuli," *Perception and Psychophysics*, Vol. 6 (6A), pp. 366-372, 1969.

31. Collins, A. A., and R. W. Cholewiak, "The shape of the vibrotactile loudness function: The effect of stimulus repetition and skin-contactor coupling," *Perception and Psychophysics*, Vol. 55 (4), pp. 465-472, 1994.

32. Fucci, D., L. Petrosino, D. Harris, and E. R. Tyler, "Exposure effects on the psychophysical scaling methods of magnitude estimation and cross-modal matching for vibrotactile stimulation of the tongue and hand," *Perceptual and Motor Skills*, Vol. 66, pp. 479-485, 1988.

33. Gescheider, G. A., K. E. Santoro, J. C. Makous, and S. J. Bolanowski, "Vibrotactile forward masking: effects of the amplitude and duration of the masking stimulus," *Journal of the Acoustical Society of America*, Vol. 98 (6), pp.3188-94, December 1995.

34. Van Doren, C. L., "The effects of a surround on vibrotactile thresholds: evidence for spatial and temporal independence in the non-Pacinian I (NPI) channel," *Journal of the Acoustical Society of America*, Vol. 87 (6), pp. 2655-61, June 1990.

35. Gescheider, G. A., A. J. Capraro, R. D. Frisina, R. D. Hamer, and R. T. Verrillo, "The effects of a surround on vibrotactile thresholds," *Sensory Processes,* Vol. 2 (2), pp. 99-115, June 1978.

36. Stephens, L. C., "Sensory Integrative Dysfunction in Young Children," *MS, OTR/L. FAOTA reprinted with permission from AAHBEI News Exchange*, Vol. 2 (1), 1997. Available: http://www.tsbvi.edu/Outreach/seehear/fall97/sensory.htm

37. Miller, L. J., and S. J. Lane, "Toward a consensus in terminology in sensory integration theory and practice: Part 1: Taxonomy of neurophysiological processes," *Sensory Integration Special Interest Section Quarterly*, Vol. 23(1), pp. 1-4, 2000.

38. Tanıdır, C., B. Güçlü, N. M. Mukaddes, and F. Ünal, *Tactile Sensitivity in Autism,* SFN 35th Annual Meeting, 2005.

39. Carey, L. M., T. A. Matyas, and L. E. Oke, "Sensory loss in stroke patients: effective training of tactile and proprioceptive discrimination," *Archives of Physical Medicine and Rehabilitation,* Vol. 74 (6), pp. 602-11, June 1993.

40. Lanzetta, M., D. Perani, D. Anchisi, B. Rosen, M. Danna, P. Scifo, F. Fazio, and G. Lundborg, "Early use of artificial sensibility in hand transplantation," *Scand J Plast Reconstr Surg Hand Surg.*, Vol. 38 (2), pp. 106-11, 2004.

Fucci, D., L. Petrosino, S. B. Schuster, and S. Wagner, "Comparison of lingual vibrotactile suprathreshold numerical responses in men and women: effects of threshold shift during magnitude-estimation scaling," *Perceptual and Motor Skills*, Vol. 70 (2), pp. 483-492, 1990.

Goodwin, A. W., and M. E. Pierce, "Population of quickly adapting mechanoreceptive afferents innervating monkey glabrous skin: Representation of two vibrating probes," *Journal of Neurophysiology*, Vol. 45, pp. 243-253, 1981.

Johansson, R. S., and A. B. Vallbo, "Spatial properties of the population of mechanoreceptive units in the glabrous skin of the human hand," *Brain Research*, Vol. 184, pp. 353-366, 1980.

Johnson, K. O., "Reconstruction of population response to a vibratory stimulus in quickly adapting mechanoreceptive afferent fiber population innervating glabrous skin of the monkey," *Journol of Neurophysiology*, Vol. 37, pp. 48-72, 1974.

Stevens, S. S., "Problems and methods of psychophysics," *Psychologial Bulletin*, Vol. 55, pp. 177-196, 1958.